Thermoelectric Devices: A Review of Devices, Architectures, and Contact Optimization

*Ran He, Gabi Schierning, and Kornelius Nielsch**

In recent years, the substantially improved performance of thermoelectric (TE) materials has attracted considerable interest in studying the potential applications of the TE technique. Serving as the bridge between TE materials and applicable TE products, TE devices must be properly designed, engineered, and assembled to meet the required performance of TE products for cooling (thermoelectric cooler) and power generation (thermoelectric generator). The principle feasibility of the TE technique has been demonstrated using a variety of different materials and processing technologies, and many different architectures of TE devices have been successfully realized. This review discusses the architectures of TE devices, including bulk and thin-film TE devices, TE devices with flexible designs, pn-junction-based TE devices that provide robust solutions for high operation temperatures, and the metamaterial-based transverse TE devices. In addition, the assembly of TE devices involves contact layers on which the reliability of TE devices depends. Thus solutions to contact issues, including bonding strength, contact resistance, and thermomechanical stress, are also reviewed.

1. Introduction

The solid-state-based thermoelectric (TE) energy conversion technique is of particular interest because of its potential application in power generation and temperature control. The possibility of converting a heat flux into an electrical current or vice versa is realized by a thermoelectric generator (TEG) or thermoelectric cooler (TEC) that employs the coupled transport between electrons and phonons. For an ideal TE device with constant TE properties, the maximum heat-to-power conversion efficiency (η_{max}) and the output power density (ω_{max}) are expressed as

$$\eta_{max} = \frac{T_H - T_C}{T_H} \cdot \frac{\sqrt{1+\overline{ZT}} - 1}{\sqrt{1+\overline{ZT}} + \frac{T_C}{T_H}} \quad (1)$$

$$\omega_{max} = \frac{(T_H - T_C)^2}{4L} \overline{\alpha^2 \sigma} \quad (2)$$

and the cooling efficiency of a TE cooling device is characterized by the coefficient of performance (COP_{max})

$$COP_{max} = \frac{T_C}{T_H - T_C} \frac{\sqrt{1+\overline{ZT}} - \frac{T_H}{T_C}}{\sqrt{1+\overline{ZT}} + 1} \quad (3)$$

where L is the length of the TE leg, and T_C and T_H are the cold-side and hot-side temperatures, respectively. The term $\overline{ZT}$ is the average value of ZT, the TE device figure of merit, between the hot and cold sides and is defined as

$$ZT = \frac{\alpha^2}{RK} T \quad (4)$$

where α, R, K, T are Seebeck coefficient, electrical resistance, thermal conductance, and absolute temperature. This device parameter also contains parasitic electrical contact resistance and thermal contact resistance (TCR). Furthermore,

$$zT = \frac{\alpha^2 \sigma}{\kappa_{ph} + \kappa_{el}} T \quad (5)$$

where σ, κ_{ph}, and κ_{el} are the electrical conductivity, phonon thermal conductivity, and electron thermal conductivity, respectively, and zT defines the respective TE materials' figure of merit. Clearly, a higher ZT corresponds to a better performance in power generation and cooling.

The thermoelectric technique is highly reliable due to their solid-state nature. There are no moving parts; therefore, the devices are quiet, scalable, and lightweight. By simply changing or reversing the current, the TEC can be applied to cooling, heating, and temperature controlling to an accuracy of ±0.001 °C. In addition, a TEG could effectively boost energy efficiency and reduce the emission of greenhouse gases by using waste heat as the power source. The applicable scenarios for TE techniques include but are not restricted to fossil-fuel power stations and engines, decay heat from radioactive materials,[1] portable camping stoves,[2] jet engines,[3] pavements,[4] the human body,[5] oil and gas pipelines,[6] etc. In fact, if necessary, the TEG may be applicable in nearly every field of industry and private life,[7] which suggests great potential or TE technique for numerous applications. Interested readers are referred to the review by Champier for more information.[7]

It was concluded by Bell that a $\overline{ZT}$ value starting at 1.5 would enable substantial waste-heat harvesting and primary power-generation applications.[8] However, up to now the performances of TE products have been inferior to competing

Dr. R. He, Dr. G. Schierning, Prof. K. Nielsch
Leibniz Institut für Festkörper- und Werkstoffforschung Dresden e.V.
Institut für Metallische Werkstoffe
Helmholtzstr. 20, 01069 Dresden, Germany
E-mail: k.nielsch@ifw-dresden.de

DOI: 10.1002/admt.201700256

© 2017 WILEY-VCH Verlag GmbH & Co. KGaA, Weinheim

techniques, and the values of $\overline{ZT}$ have been still substantially less than 1. Therefore, the application of TE products have remained limited to niche fields, such as space probes, where reliability overweighed the performance.

In the 1990s, Hicks and Dresselhaus proposed the concept for boosting zT through decreasing the dimensions of the TE material.[9,10] This concept was later confirmed in Bi_2Te_3/Sb_2Te_3 superlattices and PbTe/PbSeTe quantum dot superlattices, where a zT as high as 2.4 was claimed at room temperature.[11,12] In addition, with decreased material dimensions, high zT values were reported even in the most common semiconductors, such as Si.[13,14] These works ignited tremendous interest in exploring novel materials and new concepts for improving TE performance.[15] However, these high zT values never translated adequately into the performance of devices. Besides, the synthesis of low-dimensional materials is usually expensive and has a low yield. Therefore, the TE community actively investigated the bulk TE materials and proposed approaches, such as nanobulk structuring,[16] band convergence,[17] and resonant levels,[18] that effectively paved the way to higher zT in the material classes of chalcogenides,[16,19] skutterudites (SKUs),[20–24] half-Heusler (HH) compounds,[25–31] some silicides,[32–35] silicon–germanium alloys,[36–40] etc. Moreover, since the peak zT values of different TE materials usually appear at different temperatures, better TE performance is attainable with segmented TE legs of different TE materials that fit the respective optimal temperature range.[41–46] For example, a record high efficiency of ≈13.8% was reported by El-Genk et al. with segmented legs consisting of skutterudite and bismuth telluride.

With the improved TE materials, the importance ascends of designing and assembling the TE devices. However, in comparison with the development of TE materials, studies on TE devices are lagging. To develop high-performance TE devices, it requires not only good figure of merit (zT) of thermoelectric materials, but also satisfactory contacts, thermal interfaces, mechanical properties, interconnects, and packaging technique. Unlike TE materials where a universal quantity (zT) could be a good performance indicator, device consideration meanwhile requires a holistic approach. For instance, a lower thermal conductivity yields a higher temperature gradient and a higher internal stress due to thermal expansion; although shorter TE legs are favorable for power generation (see Eq. 2), the internal stress limits the minimum leg length below which the TE material could experience mechanical failure.[47] Hence, the thermal conductivity should be considered as a parameter to be tailored beyond simply reducing it to the lowest achievable limits, and the role of the power factor needs to be more emphasized.[48–50] Certain materials, such as half-Heusler compounds[25–30,51,52] and nanocrystalline silicon,[53,54] can provide a combination of sought for materials properties.

In this report, we review advances in TE device technologies. To clarify the nomenclature throughout this manuscript, unless otherwise specified, we refer TDG and TDC as "*TE devices* for power generation" and "*TE devices* for cooling," respectively; while we refer TEG (TEC) as "*TE products* for power generation (cooling)" that includes one or multiply TDG (TDC) integrated with heat exchangers, heat sources and heat sink and may also include control electronics. Moreover, our discussion mainly focuses on TDGs, since TDCs share the same device design as TDGs in most cases. As will be shown later, different heat sources that potentially power a TDG require a specific combination of materials that includes the TE material itself, contact materials, bonding layers, and the ceramic heat spreader. Beyond the choice of materials, the clever choice of the best TDG architecture is compulsory. The device architecture comprises the TE conversion principle itself (longitudinal and transverse TE effects, or pn-junction TDG), the adoption

Ran He currently works as a postdoc fellow at IFW-Dresden. He got his Bachelor degree in material physics in 2011 from Northeastern University, P. R. China. He studied physics at Boston College till the end of 2012, and then transferred to the University of Houston and obtained his Ph.D. degree in physics in 2016. His study mainly focuses on the transport properties of electron and phonon in mid-to-high temperature thermoelectric materials.

Gabi Schierning received her Ph.D. degree in 2005 from the University of Erlangen-Nuremberg, Germany. After postdoc positions, she then worked at the University of Duisburg-Essen and was group leader of an independent young researcher group working on nanostructured thermoelectric materials from 2009 to 2015. In 2015, she joined the Leibniz Institute for Solid State and Materials Research Dresden (IFW Dresden) as head of the department thermoelectric materials and devices.

Kornelius Nielsch has studied physics at the University Duisburg. For Ph.D. he joined the Max-Planck-Institute Halle. In 2002, he was a postdoctoral associate at MIT for one year. Before he was appointed as professor for experimental physics by Hamburg University in 2006, he has managed a research group in Halle. From 2009 until 2016 Nielsch has coordinated the German Priority Program on Nanostructured Thermoelectrics. In 2015, he became the director at the IFW Dresden.

 © 2017 WILEY-VCH Verlag GmbH & Co. KGaA, Weinheim

of the geometrical shape (cuboid or cylindrical) and size (bulk, thin film, or thick film), and its flexibility (rigid or flexible). Within this review we dedicate Section 2 to the architecture of TE devices.

It is equally important as device designing to address such issues as the reliability and lifetime of TE devices. One of the most, if not the most, critical failure mechanisms for TE devices is the strong thermomechanical stress at the interface between semiconductor and metal induced by long-term operation and thermal cycling.[55] In addition, for some TDGs, such as thin-film device, the electrical and thermal contact resistances eventually dominate and greatly limit the performance of TE devices. These problems urge the development of a corresponding contact layer for every TE material. The implemented contact layer should not only minimize the intrinsic parasitic electrical and thermal contact resistances[35,56] but also be long-term chemically and electrically stable under extreme operation conditions, especially for generators working at high temperatures.[57] A TDG cannot be applicable without successfully addressing contact issues like the mismatch of coefficients of thermal expansion (CTEs), chemical reactions, mass diffusion, etc. Extending the concepts for contact optimization summarized by Liu et al.,[58] and incorporating the most recent developments, we dedicate Section 3 to give an overview of the strategies for electrical and thermal contact design. A conclusion completes this review.

2. Architectures of TE Devices

2.1. Flat Bulk TE Device

As shown in **Figure 1**, the flat bulk TDG in its standard architecture utilizes the longitudinal Seebeck effect, where the electrical current and thermal current are parallel to each other. The TDG has the geometrical shape of a cuboid and is built from massive alternating legs of p- and n-type bulk thermoelectric materials, usually semiconductors. Typically, a stack of several metallization layers on the top and bottom of the TE legs establishes the thermal and electrical contacts. The metalized legs are assembled between two partly metalized ceramic plates such that they are electrically connected in series and thermally in parallel. Mostly, alumina (Al_2O_3)-based ceramics are hereby used and are metalized by a direct plated copper (DPC) contact structure. Aluminum nitride (AlN) ceramics that are costlier may be preferred due to its higher thermal conductivity compared with Al_2O_3. To harvest the energy, the TDG must be brought into tight-fitting contact with the heat source and the heat sink.

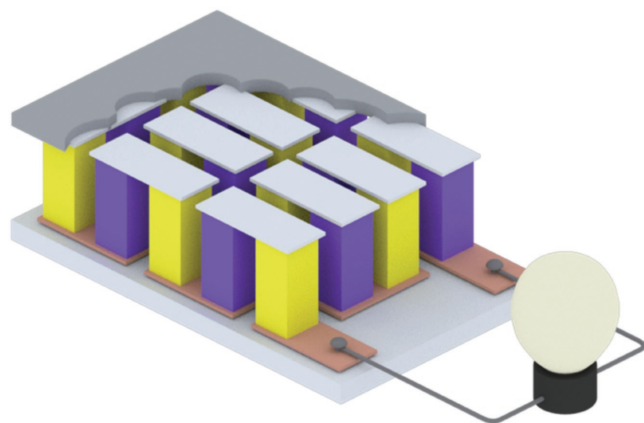

Figure 1. Conventional flat bulk architecture of a TDG. Here, the p-type and n-type semiconductor materials (yellow and purple) which comprise the active TE material are connected electrically in series using a stack of metallic contact layers. The metalized TE legs are soldered between two substrates, which are typically made of ceramics.

The manufacturing of bulk TDGs in the conventional architecture typically involves powder processing and/or sintering techniques. The ball-milling and hot-pressing approach[16,19,37] and many other means of micro- and nanostructuring the bulk material[59,60] were successfully applied to a variety of thermoelectric materials to reduce the lattice thermal conductivity and improve zT. The sintered bulk ingots are shaped by subtractive techniques, such as sawing and grinding. Typically, in a first step, the thermoelectric material is cut into wafers a few millimeters in height. Subsequently, the wafers are metalized on the top and bottom, for instance, by electrochemical plating. A second sawing process follows in which the wafers are cut into pieces that constitute the thermoelectric legs. These are picked, placed, and then soldered to the metallized ceramic plates. This process is demanding with respect to the geometrical requirements of the legs—typically several millimeters in height at an accuracy of only a few micrometers—and the resulting thermoelectric generator is mechanically rigid so that the connections to heat sink and source require less additional engineering efforts.

With certain boundary temperatures and material properties (of both TE materials and contact material), the performances of flat bulk TDGs are determined by the geometric factors including the configuration and arrangement of TE legs. To optimize the geometric factors, theoretical investigations were studied extensively, which yields the guiding principles for the actual TDG design. For example, by using smaller number of shorter legs, similar power output per unit module area can be reached as with a larger numbers of higher legs, provided that the thermal contact resistance is negligible.[61] Hodes derived expressions for calculating the number and height of TE legs that maximizes the TDG performance.[62] Besides, TE legs with various shapes such as cuboid, pyramid,[63,64] exponential,[65,66] and quadratic[67] shapes are studied and compared. The power density of TE legs are suggested higher in pyramid shape than in quadratic and exponential shapes. Recently, Mijangos et al. assembled a prototype TDG based on pyramid shaped Bi_2Te_3 TE legs.[68] Pyramidal legs (see **Figure 2**) help lowering the thermal conductance of the device so as to increase the temperature gradient along the leg, as well as harnessing the Thomson effect that is largely ignored in the traditional (cuboid) structure. The measured output power shows ≈70% enhancement in the pyramid structure than the cuboid structure, thus proving the importance of geometrical configuration of the TE legs in the device performance.

The flat bulk structure is the most discussed device architecture, and many existing TEG prototypes are built upon this architecture. Waste-heat recovery from combustion engines in

© 2017 WILEY-VCH Verlag GmbH & Co. KGaA, Weinheim

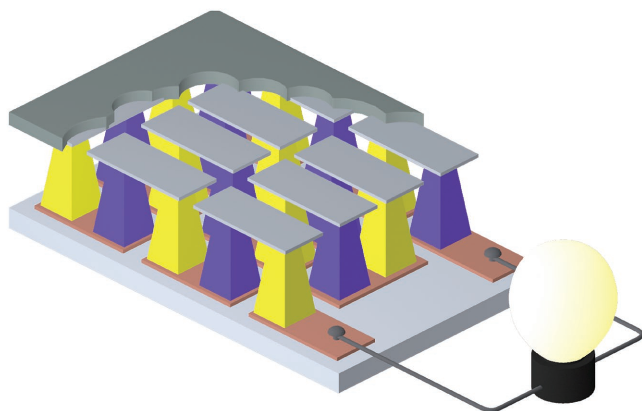

Figure 2. Flat bulk TDG with pyramidal legs to increase the temperature difference across the TE elements.

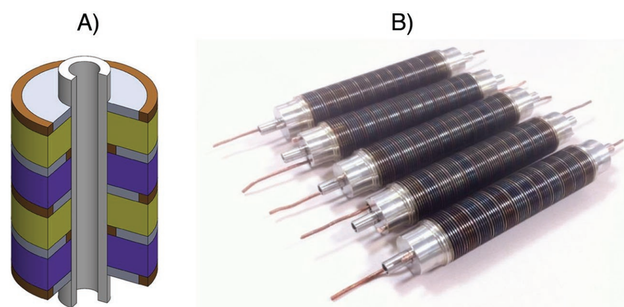

Figure 3. Cylindrical-shaped TE devices: A) design concept of the cylindrical TDC, as for instance proposed in ref. [83]. It contains the TE material (yellow and purple), the metallization layers (brownish), and isolating in-between layers. B) A cylindrical TE device. Reproduced with permission.[85] Copyright 2016, Gentherm, Eric Poliquin.

automobiles is the most discussed application of TEGs (i.e., an ATEG) based on flat bulk TDG. Most automotive efficiency studies showed the beneficial effects of ATEG integration even with the extra weight of the ATEG.[69] The hot side is heated by the waste heat or engine coolant, and the cold side of the ATEG is either cooled by engine coolant or by ambient air. Properly designed ATEGs could possibly maintain a temperature difference of hundreds of Kelvins, thus, allowing an output power as high as 1000 W.[70] Overall, an increased fuel efficiency of between 1% and 4% can be expected with the application of ATEGs.[71]

Another widely discussed flat-bulk-TDG-based TEG employs concentrated solar radiation as the heat source (i.e., a solar TEG, STEG) because of its abundance and high energy density. Since a heat exchanger is not necessary for radiative heat transfer, the STEG decreases the heat loss and enables a direct coupling between the TEG and the heat source. The efficiency (η) of an STEG is a function of the radiative flux and the radiative coupling with the converter material that needs to be tailored to reduce the reradiation effects and thermal deterioration.[72–76] Using thermal concentration, high-performance STEGs with an efficiency of up to 4.6% were demonstrated.[77,78] Recently, Kraemer et al. reported a new record conversion efficiency of ≈7.4% in an STEG.[46] To further increase the conversion efficiency of STEGs, explorations of the photo-Seebeck effect[79] or the addition of plasmonic absorbers[80] are possible routines. The photodoping effect additionally offers numerous new pathways for photothermoelectrics and deserves further investigation.[81]

2.2. Cylindrical Bulk TE Devices

Another proposed design of bulk TDGs is a cylindrical shape, as shown in **Figure 3**A.[82,83] This design is advantageous for applications such as oil pipelines, cooling channels for power station transformers, vehicle exhaust pipe, etc., where the heat flow is in the radical direction.[83] Experimentally, Schmitz et al. prepared tubular PbTe modules through a current-assisted sintering process with specially designed sintering molds.[84] In 2015, a company named Gentherm developed prototypes of cylindrical TE modules and applied them to boost the power efficiency of vehicles,[85] as shown in Figure 3B, and an output power of ≈30 W was obtainable for the individual module under optimal conditions.

2.3. Thin- and Thick-Film TE Devices

Micro-thermoelectric generators (μTDGs) and micro-thermoelectric coolers (μTDCs) have been fabricated for more than two decades for applications mostly in thermal management such as spot cooling (as for example in **Figure 4**) or for the cooling of power electronics.[86–90] The TE materials are usually designed with a thickness in the micrometer to sub-millimeter range, therefore high densities of heat flux and cooling power are attainable with the proper design of heat sink and substrate. For high-performance cooling, AlN or diamond by a chemical vapor deposition technique was used as substrate material.[91] It was discussed that μTDCs, when operated not in steady-state mode but in a transient regime, could provide even higher cooling power because of a transient cooling effect.[92,93]

Electrochemical deposition is the most preferable technique for fabricating thick-film μTE devices compared with other deposition techniques, such as evaporation or sputtering, if

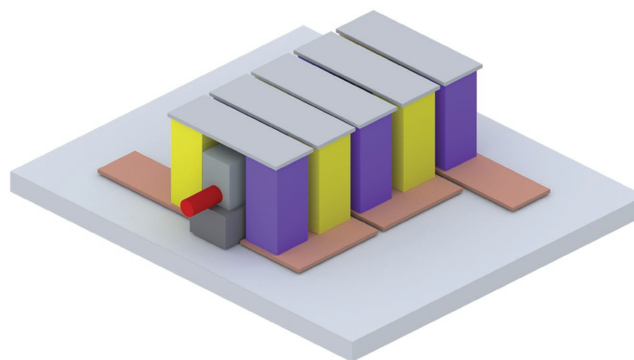

Figure 4. Schematics of an integrated μTDC for the thermal stabilization of an optical device on a wafer substrate, as envisioned by Enright et al.[88] The p-type and n-type TE legs (yellow and purple) enclose a thermal spreader, surrounding the optical component, here sketched in red.

© 2017 WILEY-VCH Verlag GmbH & Co. KGaA, Weinheim

the micrometer or sub-millimeter thick legs are deposited into cavities. In addition, it is comparatively inexpensive and compatible with complementary metal oxide semiconductor (CMOS) back-end technology. In fact, the first µTDCs from the NASA jet propulsion laboratory (Pasadena, California) utilized electrochemical deposition.[87] The electrochemical deposition of conventional TE materials has consequently been optimized by several groups.[87,94–96] A µTDG consisting of 126 TE legs of n-type and p-type $(Bi, Sb)_2Te_3$ obtained by electrochemical deposition was realized by Snyder et al.[97] They describe the fabrication of a µTDG by the sequential electrochemical deposition of n-type and p-type material on a silicon wafer. Research and development activities in this field comprise the different fabrication steps and the layout of the device.[97–101] An example for such a template-assisted local electrochemical deposition process is given in **Figure 5**.[102] The fabrication steps comprise patterning and depositing the bottom contact layer, structuring the cavities and subsequent deposition of the first TE material, structuring and subsequent deposition of the second TE material while protecting the first TE deposit, and followed by the structured deposition of the top contact (metal bridge).

Aside from electrochemical deposition methods, physical deposition methods in combination with lithographical structuring were successfully applied for µTDG/µTDC fabrication. For instance, an SiGe thin-film µTDC was realized by molecular beam epitaxy.[103] Employing sputtering methods, n- and p-type legs were processed on two separate silicon wafers that were then mechanically joined to form µTDGs by soldering or diffusion bonding.[104,105] This approach results in a planar arrangement of thermoelectric legs and a monolithic integration on one silicon substrate with precise control of the legs' height.[105] The fabrication technique is compatible with CMOS technology[106–109] and thin-film processes,[110] and requires no additional joining techniques. Planar deposition techniques were combined with fabrication processes of 3D/anical systems to achieve a modular generator platform, which is more flexible with respect to the selection of materials and geometry.[111–113]

High internal resistances on the order of, in the worst cases, up to MΩ[107,114–116] and a complex fabrication technology[114,116] are intrinsic problems of µTE devices. Typically, several lithography and deposition steps are required, sometimes additional mechanical polishing and/or handling steps, and processing is conducted mostly in clean rooms[96,101] or at least in a sufficiently clean lab environment.[102] This provides a certain obstacle to its application.

2.4. Flexible TE Devices

The fabrication of TE devices by innovative manufacturing techniques aims at mitigating the typical inflexible design and cost-intensive conventional and subtractive manufacturing techniques. The result is that TE devices are in a flexible shape. To name only the most important ones, the manufacturing techniques comprise printing, additive manufacturing, thermal spraying, melt-mixing of composites, metallurgical processing techniques, and laser-aided restructuring.

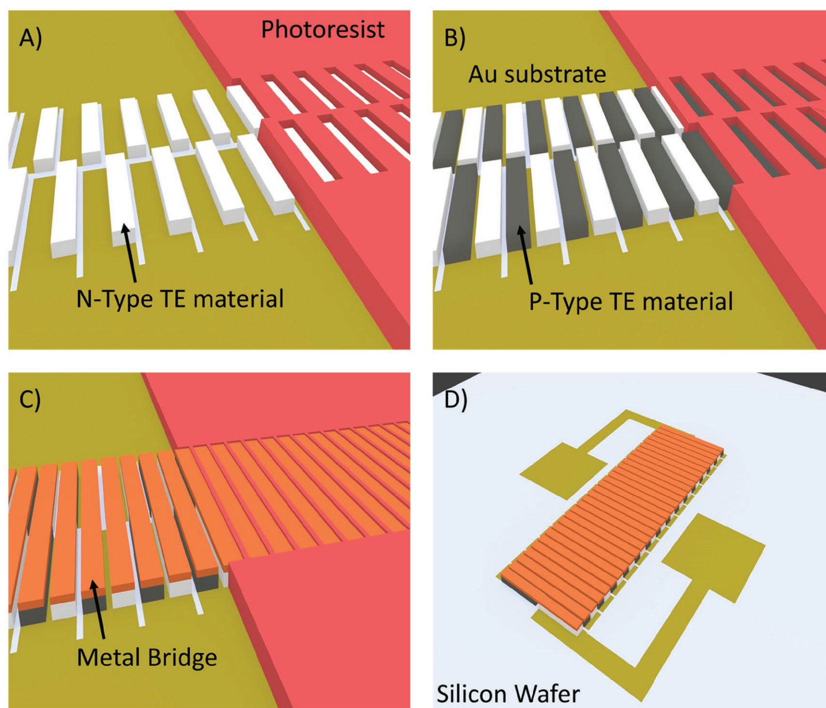

Figure 5. A–D) Schematic process flow to fabricate a µTDC, simplified and adapted from ref. [102]. A) The deposition of n-type TE material on an Au substrate, B) deposition of p-type TE material on an Au substrate, C) deposition of the metal bridge, and D) the final µTDC, after removing the superfluous Au substrate that is deposited on an Si wafer by photolithography. In panels (A)–(C), the photoresist is partially shown for better clarification.

Because of the high demand for TE materials that allow for flexible and wearable TEG concepts, a multitude of novel materials and composites with competitive TE properties has emerged in recent years. Compared with traditional TE materials, the advantages of polymers are evident: they contain abundant elements and are widely available, they are flexible and can be easily processed into different shapes, and they are also intrinsically low in density and thermal conductivity. Therefore, TE devices made from organic electronics or using composites with one organic component are currently an emerging topic, with the focus on flexible electronics.[117–123]

There are several polymers that are capable of TE applications, such as the use of intrinsically conductive polymers like poly(3,4-ethylenedioxythiophene): poly(styrenesulfonate) (PEDOT:PSS) or polyaniline (PANI). These compounds were recently proposed to be semimetals, explaining in part their good TE properties.[124,125] The TE properties of polymers could be further optimized in combination with conductive additives;[126–139] meanwhile, there are only a few attempts toward melt-mixed composites because of the low values of electrical conductivity.[140–145] Because of the poor properties of the n-type

© 2017 WILEY-VCH Verlag GmbH & Co. KGaA, Weinheim

material, organic TE devices are sometimes constructed as a single leg p-type TEG rather than the more common p- and n-type design.[146]

Flexible and foldable TE devices were also realized by embedding conducting polymers into carbon nanotube webs. Composites made of multiwall carbon nanotubes (CNTs) and PEDOT:PSS demonstrated power factors of 155 μW m^{-1} K^{-2}, competitive with lead telluride at room temperature.[147] The power factors and zT were additionally increased by decorating the composite with Au nanoparticles. A zT of ≈0.2 was obtained for Au-doped CNT/PANI, and device prototypes from these optimized webs were constructed.[148] Through properly introduced surface functionalization, both n-type and p-type properties were realized in CNT webs, with which a flexible TDG was constructed.[149] A planar TE device was realized using CNT films with a localized doping technology. Hereby, polyethylenimine (PEI) solution was locally drop casted onto the CNT film to switch the doping type from p-type to n-type, and extraordinary high power factors up to 10^{-3} W m^{-1} K^{-2} of both p-type and n-type material were achieved.[150] Similarly, an all-carbon nanotube flexible TDG was demonstrated that used a CNT-yarn, functionalized with PEI and iron chloride for n-type and p-type doping, respectively.[151] Also a graphene-based TE paper intermixed with organic and inorganic components[152] showed high flexibility and high chemical stability.

Recently, printable and/or paintable TE devices were reported and showed unique adaptabilities to random geometries of heat sources. For the printing of devices, the challenge is to ensure good electronic transport. The design of inks and pastes in terms of physical properties, such as wettability and viscosity, and the choice of proper binder and filler materials are critically important.[153] Composites of organic binder and inorganic filler constituents so far provide the best trade-offs of these partially conflicting properties, ensuring good electronic transport together with good processability. Pastes of mature TE materials, such as Bi_2Te_3 and Sb_2Te_3, were utilized in established screen printing processes, and flexible devices on Kapton foil were demonstrated.[154] In combination with epoxy, they demonstrate a room temperature zT of up to 0.4;[155,156] in another combination, with PEDOT:PSS, they approach $zT \approx 0.2$[157] and ≈0.4 after a chemical treatment.[158] By employing a hydrogen anneal on a screen-printed BiTeSe film, a zT of ≈0.9[159] was realized, and TE devices were successfully fabricated by this processing technique.[159] Furthermore, a high mechanical stability was demonstrated in solution-processed composites using plastically reinforced PEDOT:PSS together with $Bi_{0.5}Sb_{1.5}Te_3$ nanocrystals.[160] Printable pastes of chemically sintered Bi_2Te_3 achieved zTs of 0.67 and 1.21 for n- and p-type materials, respectively, with Sb_2Te_3 as the sintering aid.[161] Besides, to realize the concept of wearable TEGs using TE pastes, silk fabric was proposed as the carrier where the TE material was deposited on both sides of a silk fabric to form TE columns.[162]

Another design for flexible TE devices incorporates a 2D hybrid superlattice of TiS_2 layers and hexylamine molecules.[163] The TiS_2 layers were intercalated in the hexylamine molecules through a solution-based synthesis procedure. This design enables large-area free-standing TE foils. The obtained power factor of ≈230 μW m^{-1} K^{-2} is particularly high for a flexible TE material. A higher power factor of 450 μW m^{-1} K^{-2} and $zT \approx$ 0.28 were obtained at 100 °C in a similar design with the composition $TiS_2[(\text{hexylammonium})_{0.08}(H_2O)_{0.22}(\text{DMSO})_{0.03}]$. Such a high zT is close to the most promising p-type organic TE material, i.e., PEDOT-PSS, thus showing the robustness of the hybrid-superlattice concept.[164] Except for TiS_2, other 2D dichalcogenides, such as WS_2 or $NbSe_2$, were identified as potential materials for flexible and wearable TEGs.[165]

Figure 6 exemplarily shows some flexible TE devices. One of the first examples of a fully flexible, rolled up TDG consisting of metal films on a polyimide foil was realized by Weber et al.[166] (Figure 6A). The coiling-up of the foil yielded a high voltage on a small area and was therefore chosen as a design principle. A more recent realization of a fully flexible TDG on polyimide foil is shown in Figure 6B and uses ink-jet printing.[167] The inks consist of optimized formulations based on conventional TE nanopowders. A prototype using carbon nanotube–polystyrene composite is shown in Figure 6C.[168]

The huge variety of materials' compositions and processing opens the door for novel functionality. For instance, by immersing a porous polyurethane microstructure frame with organic TE material (PEDOT:PSS), a combined temperature and pressure sensor was demonstrated that independently senses both parameters with high accuracy under mixed stimuli.[169]

A special kind of a flexible TDG is sometimes called an "Origami" TDG (**Figure 7**A,B), which is printed on a foil in such

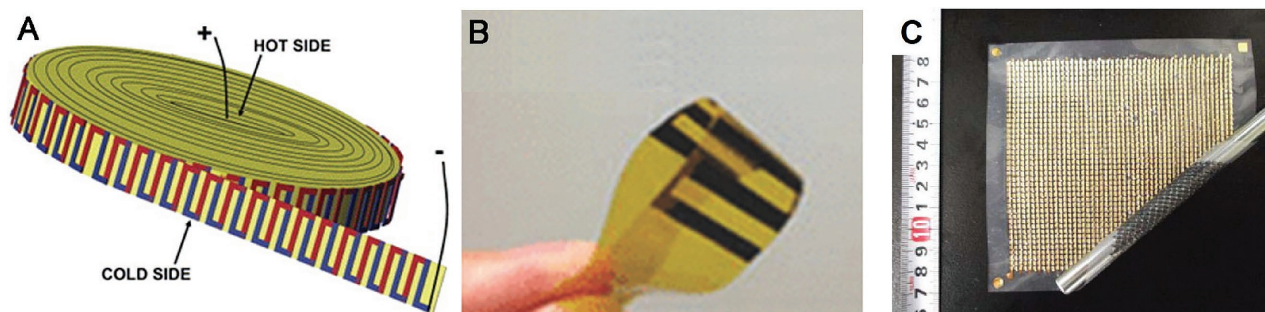

Figure 6. Flexible TE devices. A) A coin-shape coiled-up TDG. Reproduced with permission.[166] Copyright 2016, Elsevier B.V. B) A TDG foil with optimized TE inks produced by an ink-jet printing technique. Reproduced with permission.[167] Copyright 2014, WILEY-VCH Verlag GmbH & Co. KGaA, Weinheim. C) A prototype TEG using carbon nanotube–polystyrene composite. Reproduced with permission.[168] Copyright 2013, AIP Publishing LLC.

© 2017 WILEY-VCH Verlag GmbH & Co. KGaA, Weinheim

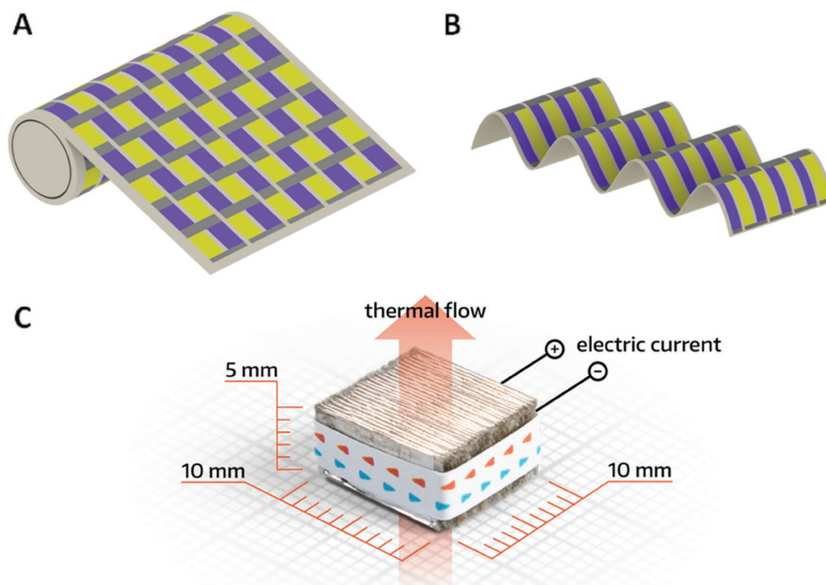

Figure 7. Origami TDG. A,B) Processing of an origami TDG that is first printed on a foil and then folded to a 3-D shape, as for instance presented in ref. [170]. C) Origami TDG by otego GmbH (Germany) to replace batteries, e.g., in thermostats. Reproduced with permission. Copyright 2017, otego GmbH.

a way that it can be shaped to fit various heat sources and heat sinks by folding.[170] A company named Otego GmbH (Germany) produces this kind of Origami TDG with the potential application to replace batteries.[171]

2.5. Wearable TDG

Wearable TDG is a special type of flexible TDG that utilizes heat from the human body.[172] Constructing wearable TDG faces distinct challenges including: i) The small working temperature difference between the body and the ambient, ii) the request to use natural air convection cooling on the cold side of the TEG, iii) the requirement of a lightweight and comforting construction, and iv) the aesthetic appeal.

The energy that a TDG can provide is defined by these constraints and by human-body heat. Several positions to integrate a wearable TDG to the human body were investigated, such as upper arm, wrist, chest, an office-style shirt,[173] or a bicycle helmet.[174] The characterization of human-body-based thermal energy harvesting resulted in a power density of ≈2.2 μW cm^{-2}, a factor of 3 less than the power density from piezoelectric based generators when the person is running at a speed of 7 miles h^{-1}.[175] However, TE devices are less affected by the state of activity of the person and generate more electrical energy in total. Usually, wearable TDG prototypes generate power on the order of a few tens of nanowatts up to a few hundreds of nanowatts.[176,177] Considering the large thermal resistances between skin/TDG and TDG/ambient interfaces, careful designs of the heat sink and heat source geometry are necessary to increase the harvested power density.[122] Although a copper heat spreader was introduced to boost the TE device performance, the low wearability limits the applicability of this design.[178] A Y-shaped fin geometry for the copper heat spreaders was shown to be efficient for application with the human body. Together with the inorganic optimized TE material, a prototype device that generated 3 μW cm^{-2} was demonstrated.[120] Additionally, a TE device integrated into a wristband was reported to yield 8.6 μW cm^{-2} by addressing the design of the copper heat spreaders.[172] The interested reader is referred to several recent reviews, dealing with specific aspects of wearable TE power generators.[179,180]

2.6. TDGs That Employ Hot-Side pn Junctions

TDGs for high operation temperatures are desirable since the conversion efficiency increases with the temperature difference across the TDG. However, the concomitant challenges at the hot-side metal–semiconductor contact such as material stability issues and thermomechanical stress have to be considered. Harsh conditions, such as extremely high temperatures, may be addressed by concepts that either dismiss the hot-side metallization or abstain from using a solid-state conversion process completely, as thermionic converters do.

As shown in **Figure 8**, the concept of a pn-junction-based TDG might eliminate hot-side metallization completely. The idea originates from the fact that the pn-junction generates electron–hole pairs at high hot-side temperatures. This design completely gets rid of contact issues between metal and semiconductor on the hot side, and therefore, shows great potential for constructing reliable and long-lifetime TE devices.

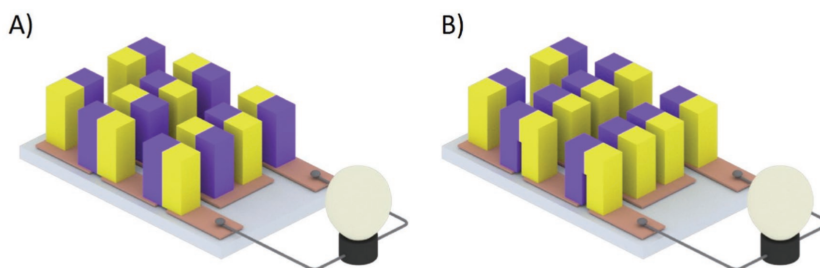

Figure 8. In a pn-TDG, the metal contact and substrate on the hot side are dismissed, and the electrical connection is made by a pn-junction of the semiconductor material. The dismissal of the metal contact and substrate on the hot side in a pn-TDG is a technological advantage. A) A pn-TDG with a large-area pn junction covering the whole length of the TE legs. B) A U-shaped TDG with "hot shoe," here with very thin isolating layer between p-type and n-type TE material, as realized in Si-Ge RTGs.[181]

© 2017 WILEY-VCH Verlag GmbH & Co. KGaA, Weinheim

To date, there are only few experimental attempts to realize this device concept. Thermopower enhancement in pn-junction arrays was reported by Zakhidov et al.[182] A direct bonding of the p-type and n-type material at the hot side was realized using polycrystalline iron disilicide to produce devices that could be operated at elevated temperature and in oxidizing atmosphere.[183,184] These devices had a U-shaped geometry and made additional use of a semiconductor–metal transition in the iron disilicide at elevated temperatures that pushed the solid bridge between p-type and n-type TE materials into a metallic state. For space missions, there was a concept specific to Si–Ge radioisotope thermoelectric generators (RTGs) that employed a so-called silicon "hot shoe" to connect the n-type and p-type legs, also forming a U-shaped couple. The p-type and n-type were still separated by a very thin glass insulating layer.[181] More recent work uses nanocrystalline silicon and a direct bonding concept to fabricate U-shaped TEGs. It was shown that a pn-junction TDG and conventional TDG, which could be made out of the same materials and by the same metallization methods, are comparable in their output power and efficiency for high hot-side temperatures.[185] Additionally, pn-junction TEGs from nanocrystalline silicon could sustain high temperatures and an oxidizing atmosphere. However, degradation mechanisms, such as the slow electromigration of the phosphorus dopant into the boron-doped leg, need to be addressed.

While the experimental work on pn-junction TDGs relies on bulk materials and the direct bonding concept, Span et al.[186,187] proposed this concept for thin-film TDGs. They argued that an enhancement of the efficiency would be possible in a pn-junction TDG compared with a conventional TDG because of additional charge carriers that are thermally induced at the hot side of the pn-junction TDG, separated within the pn junction as access carriers upon diffusion into cooler regions, and as a consequence, increased the thermocurrent through the device.

2.7. Devices with Orthogonal Flux Directions of Heat and Electrical Currents

To design a device with orthogonal flux directions of heat and electrical currents, there are two possibilities, both sketched in **Figure 9**. They have in common that the arrangement of materials and layers is carefully designed and is sometimes called a meta-material. Figure 9A hereby represents a stacking of p-type and n-type materials with an isolating layer in between.[188] The disentanglement of the electrical and thermal current directions is hereby achieved, since the electrical current is guided by the isolating layers toward the transversely arranged contacts. This arrangement corresponds to a U-shaped pn-junction TDG because of the pn junctions at the top and bottom of the meta-material, but with a very dense stacking of the p-type and n-type elements.

The dense stacking is the commonality with the device shown in Figure 9B that relies on the transverse TE effect. In most TE device architectures, the longitudinal Seebeck or Peltier effect is utilized that originates when the electrical and thermal flow are aligned in parallel. However, a transverse Seebeck or Peltier effect may occur if the electrical and thermal flow directions are perpendicular to each other. In Figure 9B, a tilted layered meta-material is used.[189] The tilting produces nonvanishing off-diagonal elements in the transport tensors that then result in the transverse TE effect. The materials' design strategy requires a highly anisotropic transport material. Often a carefully designed meta-material is utilized that consists of laminated layers or superlattices.[190–197] High transverse thermoelectric effects are hereby argued to result from atomic-layer thermopiles, for instance in $YBa_2Cu_3O_{7-\delta}$.[198] Note that the anisotropy may be enhanced by an anisotropic doping.[199] One aspect that is especially favorable using the transverse TE effect is that the geometry of the device truly represents a tuning parameter. This tuning makes use of the fact that R and K both contain geometrical dimensions that are not cancelled out in the overall device efficiency because of the different flow directions of electrical and thermal currents.[200] A Japanese team realized a bifunctional thermoelectric heat exchanger tube that employed the transverse thermoelectric effect[192,201] (**Figure 10**). They used a tilted multilayer material made of nickel and bismuth antimony telluride in the shape of a tube through which the hot fluid flows and directly provides the heat to operate the TDG.

The transverse TE effect is currently being actively explored, but its fundamental principles have long been known, as for instance reviewed by H. J. Goldsmid.[202] This paper also discusses the efficiency of devices that utilize the transverse TE effect. For $zT < 1$, the efficiency of a transverse TE device is competitive with the device that uses the longitudinal thermoelectric effects. For higher zT, the efficiency diverges, and the transverse TE devices become less competitive.[202]

3. Optimization of Contact Properties

In a TE device, the TE legs are soldered or welded to the conducting strips through bonding layers. However, the interface between the TE leg and bonding material may degrade or even breakdown in long-term high-temperature operation and

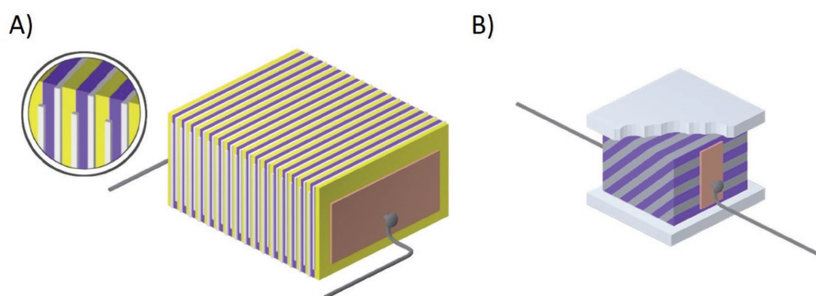

Figure 9. Device concepts that disentangle the flux directions of the heat and electrical currents in carefully designed layered materials. A) A device concept with p-type and n-type semiconductors intercalated by an isolating layer. pn Junctions guide the current flow through the material to the electrical contacts, orthogonally arranged with respect to the heat flux direction. B) A TEG employing the transverse TE effect. The material stack is composed of a semiconductor (typically highly anisotropic) and a metal and tilted to utilize the non-vanishing off-diagonal elements in the transport tensors.

© 2017 WILEY-VCH Verlag GmbH & Co. KGaA, Weinheim

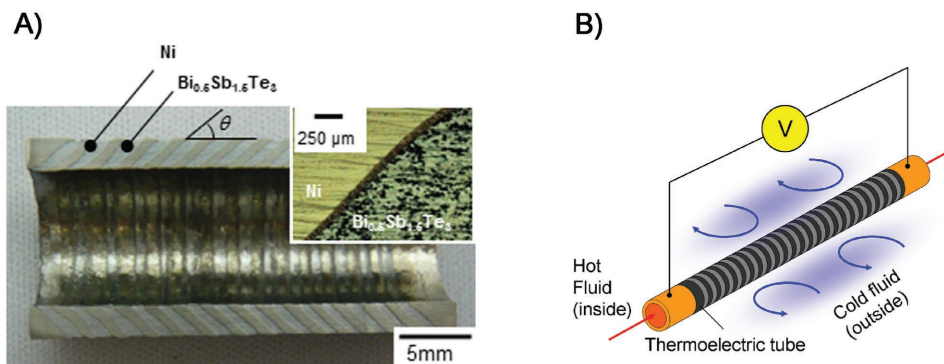

Figure 10. Tilted multilayer thermoelectric tube working as heat exchanger of nickel and BiSbTe. The bifunctional tube employs the transverse thermoelectric effect following the concept shown in Figure 9B. Original references: A) Reproduced with permission.[192] Copyright 2014, Nature Publishing Group. B) Reproduced with permission.[201] Copyright 2013, Nature Publishing Group.

during thermal cycling.[203] Possible mechanisms for the interface breakdown include the mismatch of the coefficients of thermal expansion (CTEs) of the materials in contact, mechanical embrittlement/weakening, chemical interaction and mass diffusion at interfaces, etc. In addition, the electrical and thermal contact resistances also affect the performance of TE devices. With the contact resistance, the output power (P) and conversion efficiency (η) for a TEG could be written as[82]

$$P = \frac{\alpha^2}{2\rho} \frac{AN(T_h - T_c)^2}{(n+l)\left(1+\frac{2rl_c}{l}\right)^2} \tag{6}$$

$$\eta = \left(\frac{T_h - T_c}{T_h}\right) \Big/ \left\{\left(1+\frac{2rl_c}{l}\right)^2 \left[2 - \frac{1}{2}\left(\frac{T_h - T_c}{T_h}\right) + \left(\frac{4}{ZT_h}\right)\left(\frac{l+n}{l+2rl_c}\right)\right]\right\} \tag{7}$$

where T_h and T_c are the hot-side and cold-side temperatures, respectively; N is the number of n–p pairs in a module; A and l are the cross-sectional area and the length of the TE element, respectively; and l_c is the thickness of the contact layer. The quantities n and r are defined as

$$n = 2\rho_c / \rho \tag{8}$$

$$r = \kappa / \kappa_c \tag{9}$$

where ρ_c is the electrical contact resistivity, and κ_c is the thermal contact conductivity. Clearly, a low contact resistance is favorable for increasing the device performance.

Therefore, for many TE devices, depending on the specific problems from case to case, a stack of multiple layers is usually necessary to tune the CTE mismatch, inhibit mass diffusion, or reduce the contact resistance. As shown in **Figure 11**, the assembly of TE devices usually involves the development of a proper contact material that is located between the TE materials and the bonding layer. A good contact layer should satisfy the following criteria: (1) High electrical and thermal conductivities to minimize the internal electrical and heat power losses. (2) A high ductility to be worked into a thin layer. (3) Low (electrical and thermal) contact resistances with the TE material. (4) High mechanical and thermal stabilities to be able to withstand external high temperatures and thermal shock. (5) A similar coefficient of thermal expansion to that of the TE material. (6) High chemical stability and high bonding strength with the TE leg.

In most cases, metals or metal alloys are employed as the contact layers, therefore, criteria (1), (2), and (4) are mostly satisfied. However, careful design and engineering are necessary to meet the requirements of the remaining three criteria, i.e., CTE match, chemical interaction, and contact resistance.

3.1. Matching of CTEs

The reliability of TE devices is of utmost importance since the TE devices are often applied where reliability overweighs the conversion efficiency or when the application scenarios forbid maintenance upon device failure, such as deep space probes and nuclear plants. One important requirement of device reliability is the mechanical robustness under the externally applied

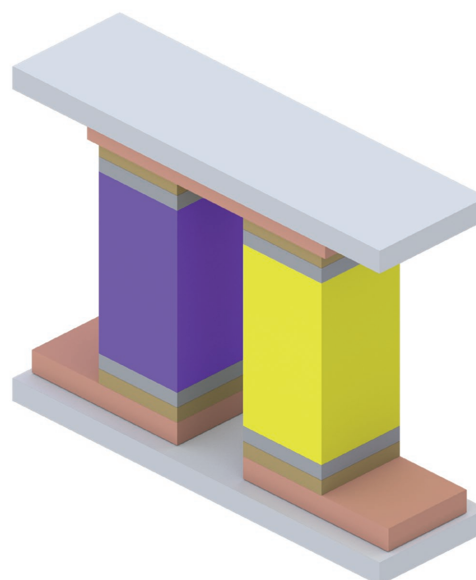

Figure 11. Configuration of a TE unicouple consisting of p-type and n-type legs (yellow and purple). The contact layer is located between the TE leg and the solder layer and bonds to the conducting strip.

© 2017 WILEY-VCH Verlag GmbH & Co. KGaA, Weinheim

mechanical or thermal stresses upon thermal cycling.[55] Ravi et al. concluded that the matching of CTEs is critically important for the development of long-life thermoelectric modules by a thermomechanical stress analysis using finite-element modelling.[204] Significant stress between the contact layer and the TE element resulting from a large CTE mismatch could yield a higher risk of the in situ fracture of the device.[58] Therefore, the thermally mismatched systems require careful engineering to meet performance expectations such as long-term survivability.

The values of CTE vary significantly among the commonly studied TE materials: ≈8–12 ppm K^{-1} for half-Heusler (MCoSn- and MNiSn-based, M = Hf, Zr, Ti),[205] ≈7.5 ppm K^{-1} for Mg_2Si,[206] ≈3–6 ppm K^{-1} for SiGe alloys,[207,208] ≈10–12 ppm K^{-1} for n-type skutterudites, 13–15 ppm K^{-1} for p-type skutterudites,[204,209,210] ≈17 ppm K^{-1} for p-type $Yb_{14}MnSb_{11}$,[204] 8–14 ppm K^{-1} for Bi_2Te_3,[211,212] ≈20 ppm K^{-1} for PbTe,[213,214] ≈21–24 ppm K^{-1} for LAST,[215] and ≈14 ppm K^{-1} for clathrates.[216] The corresponding contact layers should match the CTE of different TE materials. One effective approach for CTE matching is varying the composition in the contact layer that is sensitive to the elemental ratio. For example, a W–Cu alloy was employed as the contact material for skutterudites ($CoSb_3$), and different W/Cu ratios yield different CTE.[210] The CTE of $W_{90}Cu_{10}$, $W_{85}Cu_{15}$, and $W_{80}Cu_{20}$ are ≈6, ≈8, and ≈10 ppm K^{-1}, respectively, meanwhile the CTE of $CoSb_3$ is ≈11 ppm K^{-1}. Therefore, $W_{80}Cu_{20}$ is applicable as the contact material for $CoSb_3$. Indeed, among the three compositions ($W_{90}Cu_{10}$, $W_{85}Cu_{15}$, and $W_{80}Cu_{20}$), only $W_{80}Cu_{20}$ successfully bonded to the TE leg without cracking during thermal cycling.[210]

Another effective approach is applying multiple contact layers that have gradually varying CTEs. This was demonstrated by Singh et al., where Fe was employed as the contact layer for PbTe-based TE modules.[217] Because of the considerable difference in the CTEs of Fe (≈12 ppm K^{-1}) and PbTe (≈20 ppm K^{-1}), an extra layer of 50% Fe + 50% PbTe was inserted between the Fe and PbTe. This design allowed for a smooth transition of the CTE and resulted in a higher thermal mismatch toleration; however, also inevitably increased the contact thickness and subsequently yielded higher thermal and electrical losses. A possible alternative that does not require an extra layer is employing the metal–matrix composite that contains at least two constituent parts: the matrix necessarily being a metal, such as Cu, and the other material possessing a negative coefficient of thermal expansion (NTE). The CTE of the hybrid structure is largely tuneable by changing the amount of the NTE component. For example, Shan et al. suggested a contact material with a tuneable CTE by constructing a metal–matrix composite of Cu and La(Fe, Si, Co)$_{13}$, where the latter possesses an NTE of −37.1 ppm K^{-1} in the range of 290–327 K.[218] With mass fractions of Cu at 12.5, 25, 37.5, 50, and 60 wt%, the CTE of the composites were −23.4, −14.3, −10.1, −4.2, and 4.1 ppm K^{-1}, respectively. A tuneable CTE allows for the design and realization of the desired CTE.

3.2. Bonding Strength and Interface Reactions

With the operation of TE legs at high temperatures, the chemical interaction between the TE leg and the contact layer is inevitable. A slight chemical reaction can be favorable to increase the bonding strength. However, a severe chemical reaction might lead to increased contact resistance and the subsequent degradation of thermoelectric performance, which causes reliability problems during high-temperature operation.[219,220] In addition, cracks and voids are also commonly observed when the reaction products are brittle.[213,221,222] Therefore, the favorable extent of a chemical reaction should be balanced between the mechanical (bonding strength) and electrical (contact resistance) considerations.

For example, Liu et al. studied the contact properties between Ni and n-type $Bi_2Te_{2.7}Se_{0.3}$ or p-type $Bi_{0.4}Sb_{1.6}Te_3$.[219] The contact was fabricated through the direct hot pressing of the sandwiched powders of Ni/$Bi_2Te_{2.7}Se_{0.3}$/Ni or Ni/$Bi_{0.4}Sb_{1.6}Te_3$/Ni. As shown in **Figure 12**, the final products showed a clear interface reaction layer (IRL) between the TE leg and contact material. For n-type $Bi_2Te_{2.7}Se_{0.3}$, the thickness of the IRL increased dramatically from ≈4 to ≈20 µm with hot-pressing temperatures of 400 and 500 °C, respectively. Similarly, the IRL thickness of p-type $Bi_{0.4}Sb_{1.6}Te_3$ increased from ≈3 to ≈15 µm for the same increase in hot-pressing temperature. Such an IRL was formed through the diffusion of Ni along the grain boundary. Benefiting from the formation of the IRL, satisfying bonding strengths of ≈20 and ≈30 MPa were obtained for contacts with Ni/$Bi_{0.4}Sb_{1.6}Te_3$ and the Ni/$Bi_{0.4}Sb_{1.6}Te_3$, respectively.

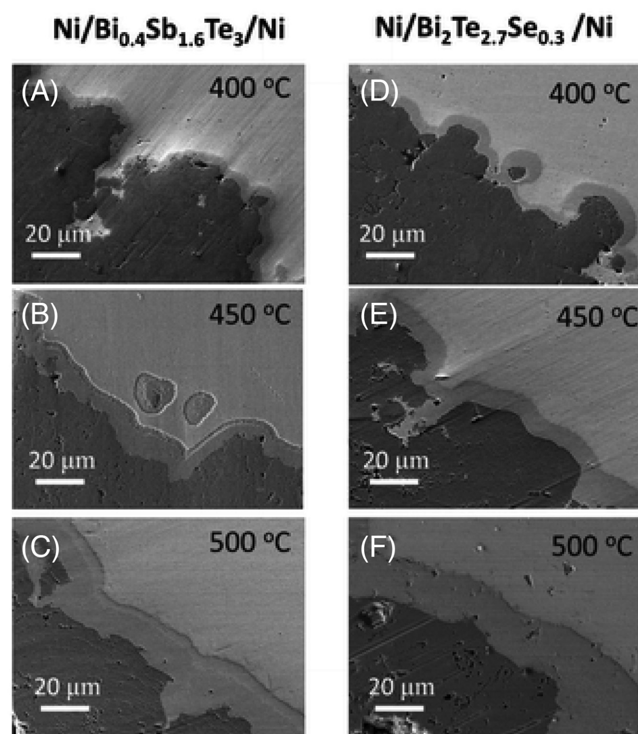

Figure 12. Microstructures of the contact interface made by directly hot pressing the Ni powders and TE powders together: A) Ni/BiSbTe/Ni, hot pressed at 400 °C; B) Ni/BiSbTe/Ni, hot pressed at 450 °C; C) Ni/BiSbTe/Ni, hot pressed at 500 °C; D) Ni/BiTeSe/Ni, hot pressed at 400 °C; E) Ni/BiTeSe/Ni, hot pressed at 450 °C; F) Ni/BiTeSe/Ni, hot pressed at 500 °C. The dark region is nickel, and the bright region is a TE material. BiSbTe: $Bi_{0.4}Sb_{1.6}Te_3$; BiTeSe: $Bi_2Te_{2.7}Se_{0.3}$. Reproduced with permission.[219] Copyright 2013, Royal Society of Chemistry.

© 2017 WILEY-VCH Verlag GmbH & Co. KGaA, Weinheim

In comparison, the bonding strength was only ≈11 MPa with the insertion of a barrier layer of Ni_3Te_2 and Ni_2Te_3, which prevents the Ni diffusion. However, the diffusion of Ni yielded the formation of a p-type region within the n-type $Bi_2Te_{2.7}Se_{0.3}$ during the hot-pressing process, since Ni is a p-type dopant for Bi_2Te_3.[219] The formed p-type region subsequently led to a large contact resistance (≈210 μΩ cm^2) for the n-type Ni/$Bi_2Te_{2.7}Se_{0.3}$/Ni, while in the p-type Ni/$Bi_{0.4}Sb_{1.6}Te_3$/Ni, the contact resistance was substantially smaller (<1 μΩ cm^2).

The tradeoff between the electrical and mechanical requirements of the contacts can be tuned by introducing a barrier layer. For example, the contact between Fe and TAGS-85 ($(AgSbTe_2)_{0.15}(GeTe)_{0.85}$) degrades significantly due to the diffusion of Fe into the TE leg.[223] The diffusion of Fe results in an increase of contact resistance and the loss of device strength. By introducing SnTe as the barrier layer, Singh et al. reported no observation of diffusion across Fe/SnTe or SnTe/TAGS-85 interfaces, thus, both the bonding strength and the contact resistance were satisfyingly preserved.[217] However, the insertion of a barrier layer increases the loss of electric and thermal flows, thus, decreasing the conversion efficiency of TE devices.

3.3. Thermal Contact Resistance

The TCR yields a finite discontinuity of the temperature profile across the contact boundary. In general, the lower the TCR, the higher the TE device performance. In one special case where the contact layer is thermoelectrically nontrivial, a higher TCR could possibly enhance the device performance.[224] Yamashita quantitatively showed that if the Seebeck coefficient of the contact interface reaches half the value of the TE material, a higher TCR might improve the COP for a TE cooler.[225] With a high TCR, the temperature drop across the contact interface contributes to the voltage output due to the boundary Seebeck effect. This is an interesting concept, yet there is no experimental proof to our best knowledge. For the design of most TE modules, seeking contact layers with low TCR is still more prevailing and practical.

The TCR has two usual origins: 1) surface asperities and 2) the Kapitza resistance. The surface asperity yields decreased contact area because of the roughness of the contacting surfaces at the microscopic scale.[226] Quite often the random geometry of surface asperities can be minimized through the fine polishing of the contact surfaces to effectively increase the contact area to suppress the TCR. On the other hand, the Kapitza resistance originates from the differences in the vibrational properties across the contact. The probability of phonons being back scattered up on striking the boundary is related to the density of states and phonon speeds of different modes on both sides of the boundary, which are independent of the surface asperities.[227] The TCR is an intrinsic problem of every TEG but becomes especially challenging for generators that need to manage high energy fluxes, such as thin-film TEGs. For many bulk TE devices, the contact layer is usually directly sintered together with the TE leg. Therefore, surface asperity is usually not a big problem between the TE legs and the contact layers. Meanwhile, to suppress the Kapitza resistance, one possible approach was proposed by English et al. stating that if the interfaces are geometrically well defined, the concept of phonon bridges might be applicable to mitigate the TCR (**Figure 13**): A phonon bridge has a spectral density of states (DOS) that eases the transfer of phonons from one side of the interface to the other.[228]

3.4. Electrical Contact Resistance

The electrical contact resistance in the metal–semiconductor junction is one of the oldest issues to be addressed in semiconductor-based devices. For TE devices, the TE legs are usually semiconductors, while the contact layer is usually a metal to minimize the electric and thermal losses. Depending on the formation of the junction, metal–semiconductor contacts can possess a rectifying (Schottky) or nonrectifying (ohmic) behavior. Therefore, the metal–semiconductor junction has to be properly designed so that electrical charges can be conducted easily.

The subject of metal–semiconductor contact formation is too broad to be discussed in detail here. The interested reader should refer to specific references for details.[229–231] Ideally, if the contact surfaces are clean and possess sharp profiles of atoms, the contact resistance is determined by the work function of the metal (ϕ_M) and the electron affinity (χ_{SC}) of the semiconductor. Here, we define that if ϕ_M is larger than χ_{SC}, the metal is referred to as high work-function metal. Contrarily, a low work-function metal means ϕ_M is smaller than χ_{SC}. Principally, to build ohmic contact behaviour, metals with a low (high) work function are favorable for contacting n-type (p-type) semiconductors. However, this assumption is oversimplified,

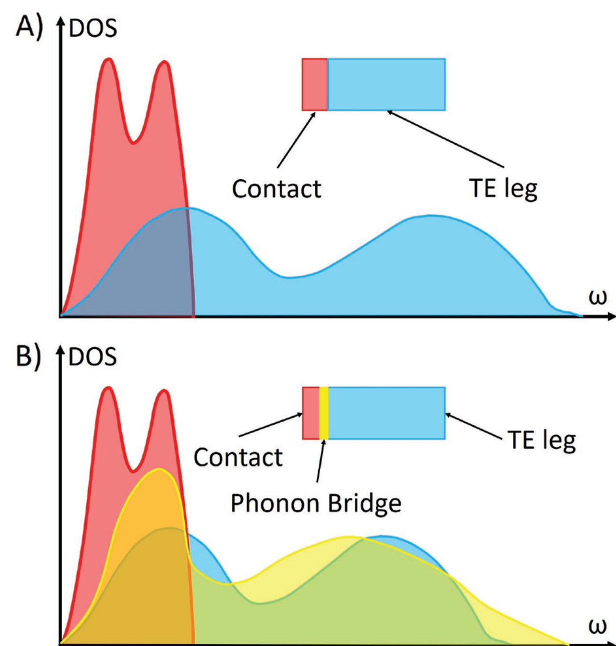

Figure 13. Schematics showing the concept of Phonon Bridge, as suggested in ref. [228]. A) the mismatching of phonon DOS between contact layer and TE leg, B) an intermediate layer that adjusts the spectral DOS to optimize the transfer of phonons across the interface.

© 2017 WILEY-VCH Verlag GmbH & Co. KGaA, Weinheim

and a more realistic boundary region can be treated as a dipole layer with a finite length scale (usually on the order of several Å) because of the charge flow for the Fermi-level alignment. In addition, a thin layer of new compound usually forms due to the chemical reaction at the contact. Therefore, one can expect the formation of new electronic interface states. With the presence of interface states, as proposed by Bardeen,[232] the density of states (DOS) increases at the Fermi level, which effectively pins the Fermi level in the interface states. The Fermi-level pinning effect induced by interface states is unfavorable for TE devices, since it preserves the Schottky barrier height. It was proposed that covalent semiconductors have a high interface state density so that the barrier height is essentially independent of the metal; meanwhile, ionic semiconductors exhibit a low density of interface states, therefore, their barrier height is strongly dependent on the metal.[233,234]

Among the state-of-the-art TE materials, oxides, half-Heusler compounds, MgAgSb, TAGS, and Zintl phases are more ionic, while for SiGe, $CoSb_3$, PbTe, and Bi_2Te_3, the chemical bonds are more covalent. The variety of TE materials requires different solutions to achieve a satisfying contact. In the following sections, we present the contact designs of several well-studied TE materials.

3.4.1. Skutterudite

The contact material of SKU was studied broadly due to its prospective potential application at mid-temperatures, such as with waste heat from vehicles. Here, we list some of the contact designs with the electrical contact resistance in parentheses (if available): $Ti/Ce_{0.85}Fe_{3.5}Co_{0.5}Sb_{12}$ (<5 μΩ cm^2);[44] $Mo–Cu/Ti/CoSb_3$ (20–30 μΩ cm^2);[221,235] $Nb/Cu_{28}Ag_{72}/CoSb_3$ (<5 μΩ cm^2);[236] $W–Cu/Ti/CoSb_3$ (<50 μΩ cm^2);[210] $Ti/Zr/CoSb_3$ (19 μΩ cm^2);[237] Co–Fe–Ni alloy/SKU;[238] $Co_2Si/NdFe_{3.5}Co_{0.5}Sb_{12}$ and $CoSi_2/Yb_{0.35}Co_4Sb_{12}$ (1 to ≈2 μΩ cm^2).[239] Among these designs, Ti-based and Zr-based contacts suffer from chemical interactions during aging, thus, they are not promising candidates as a contact material.

In 2015, a patent filed by Jie et al. reported the contact behavior between the p-type skutterudite $Ce_{0.45}Nd_{0.45}Fe_{3.5}Co_{0.5}Sb_{12}$ and a Cr–Fe–Co or Cr–Fe–Ni alloy.[240] They reported that the matching of the electronic work function of the alloy with the filled skutterudite played a crucial role in determining the electrical contact resistance. The sensitivity of the contact resistance to the work-function matching allowed an extremely low contact resistance (≈0.4 μΩ cm^2). Their work demonstrated that work-function matching is an effective guiding principle for choosing the right contact material for thermoelectric materials in general, as long as there is no severe reaction occurring in between.

3.4.2. SiGe Alloy

One of the most notable applications of the TE technique is the RTG that was employed for space probes. In some of the RTGs, SiGe alloys were employed as the TE leg to match an application temperature of up to 1000 °C. The diagrams of the RTG show the contact designs using silicon–molybdenum (Si–Mo) compounds on the hot side, while multiple Cu–W layers were used on the cold side.[241] However, the detailed composition of the Si–Mo compounds was not clear. Lin et al. reported the fabrication of an $(Si–MoSi_2)$/SiGe junction, but the reported contact resistivity exceeded 2000 μΩ cm^2, which is too high to be applicable.[242] Another work done by Lin et al. employed a $W–Si_3N_4$ electrode for SiGe with $TiB_2–Si_3N_4$ or $MoSi_2–Si_3N_4$ as an intermediate layer via a hot isostatic pressing process.[243] Although the contact resistivity was still large (>100 μΩ cm^2), the contact of $W–Si_3N_4/TiB_2–Si_3N_4$/SiGe is promising due to the similar CTEs of tungsten (≈4.5 ppm K^{-1}) and SiGe (≈4.2 ppm K^{-1}). As a compound with high electrical and thermal conductivities, the TiB_2 interlayer not only minimized the energy loss but also effectively prevented the interdiffusion of W and SiGe. In addition, through the mixing of Si_3N_4 into W and TiB_2, a better CTE matching was realized since Si_3N_4 has a smaller CTE (2.5–3.0 ppm K^{-1}). Therefore, by fine tuning the content of Si_3N_4 in the $TiB_2–Si_3N_4$ layer, optimized CTE matching and contact resistance were attainable. The recent work of Yang et al. showed that with the contact design of $W_{0.7}(Si_3N_4)_{0.3}$–$(TiB_2)_{0.8}(Si_3N_4)_{0.2}$–$Si_{80}Ge_{20}B_{0.6}$, a suppressed contact resistance of ≈75 μΩ cm^2 was obtained.[244] The contact resistance was maintained even after ageing for 120 h at 1000 °C, showing its application potential.[244]

3.4.3. Bi_2Te_3

Depending on the application purposes of Bi_2Te_3-based TE devices, either for cooling or power generation, the contact solutions are different. For cooling applications, usually a thin layer of Ni with a thickness of 0.5–1 μm is coated on the Bi_2Te_3 legs either through sputtering[245] or electroplating,[246] followed by a protective layer of copper or gold for soldering tin.[245,246] For power generation applications of Bi_2Te_3-based TE devices, the main issue of designing the contact is the balance between bonding strength and contact resistance.[219] Furthermore, the Ni barrier layer needs to be significantly thicker to prevent interdiffusion because of the relatively higher application temperature.[247,248] In addition, the insertion of Cr or a Ta–Si–N alloy was also reported as effective buffer layers to prevent the atomic diffusion of the contact.[249–251] By directly hot pressing Ni powder onto Bi_2Te_3 powder, Liu et al. observed the formation of a p-type region in the n-type $Bi_2Te_{2.7}Se_{0.3}$ because of the diffusion of Ni. The p-type region significantly increased the contact resistance by two orders of magnitude. This problem was partially solved by using a buffer layer such as $NiSe_2$ or $(Bi_2Te_{2.7}Se_{0.3})_{0.99}(SbI_3)_{0.01}$ that effectively suppresses the contact resistance (1 μΩ cm^2) while maintaining a decent bonding strength (16 MPa).[219]

3.4.4. PbTe

For PbTe-based TE devices, an Fe contact layer is the most common option.[217] The contact resistance between Fe and PbTe can be as low as ≈7.2 μΩ cm^2. The only problem with Fe is the CTE mismatch, where the CTEs of PbTe and Fe are ≈20 ppm K^{-1} and 12 ppm K^{-1}, respectively. The solution to the

© 2017 WILEY-VCH Verlag GmbH & Co. KGaA, Weinheim

CTE mismatch usually relies on an intermediate layer of mixed Fe and PbTe.[217,252] Another applicable contact layer for PbTe is Ni. The CTE of Ni (≈13.4 ppm K^{-1}) is higher than that of Fe, and the high contact resistance between Ni and PbTe can be reduced by the insertion of an SnTe layer.[253]

3.4.5. Half-Heusler

The contact design for HH-based compounds is relatively straightforward. A patent by Joshi et al.[254] and papers by Zhang et al.[255] and He et al.[52] reported contact on the hot side by simply brazing HH legs to the Cu electrode using a Zn–Cd-based or Cu–Ag-based alloy. On the cold side, the TE legs were soldered to the Cu electrode using $In_{52}Sn_{48}$. The obtained contact resistance was smaller than 1 μΩ cm^2, while the bonding strength was as high as ≈40 MPa.[255] This design was proven effective for p-type MCoSb-, p-type NbFeSb-, and n-type MNiSn-based compounds,[51] therefore successfully addressed the contact issue for HH compounds.

4. Summary and Outlook

To realize the application of TE conversion techniques, problems regarding the design and assembly of TE devices have to be addressed. In this review, we summarize the architectures of TE devices including bulk and thin-film TE devices, flexible and wearable TE devices, pn-junction-based TE devices, and metamaterial-based transverse TE devices. Suitable device architectures have to be selected to adapt many considerations such as heat–sink and heat–source temperatures, geometry matching, and performance optimization. Meanwhile, reliability is greatly required for TE devices. Hence, we discuss issues at the contacts of TE devices since they are a highly failure-prone region. The problems are summarized as the matching of coefficients of thermal expansion, chemical reactions, and contact resistance. Contact solutions for several TE materials are also reviewed.

Despite the recent development in TE devices and their promising potentials for applications, substantial work remains to be done to translate the high performance of TE materials to advanced TE devices. We emphasize the fact that to this day, commercially available TE products are limited to only few TE materials, applied at low temperature (≈225 °C at hot junction for TEG), and the discovery of new higher performance TE materials has not much translated into practical applications largely due to the low maturity level of device technologies. It is of great importance for the TE community to focus on addressing the device-level challenges and assembling pragmatic and convincing TE products in a timely fashion.

Keywords

contact, device architectures, thermoelectric coolers, thermoelectric devices, thermoelectric generators

Received: September 17, 2017
Revised: October 27, 2017
Published online:

[1] T. R. Barker, W. L. Kershaw, G. S. Stivers, J. L. Thomas, *US3615869 A*, **1971**.
[2] M. Rahman, R. Shuttleworth, *Pro. Inter. Conf. Energy Manag. Power Delivery*, **1995**, *1*, 186.
[3] C. Bode, J. Friedrichs, R. Somdalen, J. Köhler, K.-D. Büchter, C. Falter, U. Kling, P. Ziolkowski, K. Zabrocki, E. Müller, D. Kožulović, *ASME 2016 International Mechanical Engineering Congress and Exposition*, *Volume 1: Advances in Aerospace Technology*, Phoenix, Arizona, USA, (accessed: November 2016).
[4] L. Guo, Q. Lu, *Renewable Sustainable Energy Rev.* **2017**, *72*, 761.
[5] M. Hyland, H. Hunter, J. Liu, E. Veety, D. Vashaee, *Appl. Energy* **2016**, *182*, 518.
[6] J. C. Bass, R. L. Farley, *Proceedings of the 16th International Conference on Thermoelectrics (ITC)*, **1997**, 547.
[7] D. Champier, *Energy Convers. Manage.* **2017**, *140*, 167.
[8] L. E. Bell, *Science* **2008**, *321*, 1457.
[9] L. D. Hicks, M. S. Dresselhaus, *Phys. Rev. B* **1993**, *47*, 12727.
[10] L. D. Hicks, M. S. Dresselhaus, *Phys. Rev. B* **1993**, *47*, 16631.
[11] R. Venkatasubramanian, E. Siivola, T. Colpitts, B. O'Quinn, *Nature* **2001**, *413*, 597.
[12] T. C. Harman, *Science* **2002**, *297*, 2229.
[13] A. I. Hochbaum, R. Chen, R. D. Delgado, W. Liang, E. C. Garnett, M. Najarian, A. Majumdar, P. Yang, *Nature* **2008**, *451*, 163.
[14] A. I. Boukai, Y. Bunimovich, J. Tahir-Kheli, J.-K. Yu, W. A. Goddard III, J. R. Heath, *Nature* **2008**, *451*, 168.
[15] W. Liu, J. Hu, S. Zhang, M. Deng, C.-G. Han, Y. Liu, *Mater. Today Phys.* **2017**, *1*, 50.
[16] B. Poudel, Q. Hao, Y. Ma, Y. Lan, A. Minnich, B. Yu, X. Yan, D. Wang, A. Muto, D. Vashaee, X. Chen, J. Liu, M. S. Dresselhaus, G. Chen, Z. Ren, *Science* **2008**, *320*, 634.
[17] Y. Pei, X. Shi, A. LaLonde, H. Wang, L. Chen, G. J. Snyder, *Nature* **2011**, *473*, 66.
[18] J. P. Heremans, V. Jovovic, E. S. Toberer, A. Saramat, K. Kurosaki, A. Charoenphakdee, S. Yamanaka, G. J. Snyder, *Science* **2008**, *321*, 554.
[19] Y. Lan, B. Poudel, Y. Ma, D. Wang, M. S. Dresselhaus, G. Chen, Z. Ren, *Nano Lett.* **2009**, *9*, 1419.
[20] S. Ballikaya, C. Uher, *J. Alloys Compd.* **2014**, *585*, 168.
[21] G. Rogl, A. Grytsiv, P. Rogl, E. Bauer, M. Zehetbauer, *Intermetallics* **2011**, *19*, 546.
[22] G. Rogl, A. Grytsiv, P. Rogl, N. Peranio, E. Bauer, M. Zehetbauer, O. Eibl, *Acta Mater.* **2014**, *63*, 30.
[23] Q. Jie, H. Wang, W. Liu, H. Wang, G. Chen, Z. Ren, *Phys. Chem. Chem. Phys.* **2013**, *15*, 6809.
[24] T. Dahal, Q. Jie, W. Liu, K. Dahal, C. Guo, Y. Lan, Z. Ren, *J. Alloys Compd.* **2015**, *623*, 104.
[25] M. Schwall, B. Balke, *Phys. Chem. Chem. Phys.* **2013**, *15*, 1868.
[26] K. Bartholome, B. Balke, D. Zuckermann, M. Koehne, M. Mueller, K. Tarantik, J. Koenig, *J. Electron. Mater.* **2014**, *43*, 1775.
[27] F. Casper, T. Graf, S. Chadov, B. Balke, C. Felser, *Semicond. Sci. Technol.* **2012**, 27.
[28] X. Yan, W. Liu, H. Wang, S. Chen, J. Shiomi, K. Esfarjani, H. Wang, D. Wang, G. Chen, Z. Ren, *Energy Environ. Sci.* **2012**, *5*, 7543.
[29] S. Chen, Z. Ren, *Mater. Today* **2013**, *16*, 387.
[30] G. Joshi, T. Dahal, S. Chen, H. Z. Wang, J. Shiomi, G. Chen, Z. F. Ren, *Nano Energy* **2013**, *2*, 82.
[31] G. Joshi, R. He, M. Engber, G. Samsonidze, T. Pantha, E. Dahal, K. Dahal, J. Yang, Y. Lan, B. Kozinsky, Z. Ren, *Energy Environ. Sci.* **2014**, *7*, 4070.
[32] M. B. A. Bashir, S. Mohd Said, M. F. M. Sabri, D. A. Shnawah, M. H. Elsheikh, *Renewable Sustainable Energy Rev.* **2014**, *37*, 569.
[33] S. Battiston, S. Fiameni, M. Saleemi, S. Boldrini, A. Famengo, F. Agresti, M. Stingaciu, M. S. Toprak, M. Fabrizio, S. Barison, *J. Electron. Mater.* **2013**, *42*, 1956.

© 2017 WILEY-VCH Verlag GmbH & Co. KGaA, Weinheim

[34] S. K. Bux, M. T. Yeung, E. S. Toberer, G. J. Snyder, R. B. Kaner, J.-P. Fleurial, *J. Mater. Chem.* **2011**, *21*, 12259.
[35] J. de Boor, C. Gloanec, H. Kolb, R. Sottong, P. Ziolkowski, E. Müller, *J. Alloys Compd.* **2015**, *632*, 348.
[36] C. B. Vining, *J. Appl. Phys.* **1991**, *69*, 331.
[37] G. Joshi, H. Lee, Y. Lan, X. Wang, G. Zhu, D. Wang, R. W. Gould, D. C. Cuff, M. Y. Tang, M. S. Dresselhaus, G. Chen, Z. Ren, *Nano Lett.* **2008**, *8*, 4670.
[38] X. W. Wang, H. Lee, Y. C. Lan, G. H. Zhu, G. Joshi, D. Z. Wang, J. Yang, A. J. Muto, M. Y. Tang, J. Klatsky, S. Song, M. S. Dresselhaus, G. Chen, Z. F. Ren, *Appl. Phys. Lett.* **2008**, *93*, 193121.
[39] A. Kallel, G. Roux, T. Derycke, C. L. Martin, M. Marinova, C. Cayron, *AIP Conf. Proc.* **2012**, *1449*, 409.
[40] Z. Zamanipour, X. Shi, A. M. Dehkordi, J. S. Krasinski, D. Vashaee, *Phys. Status Solidi A* **2012**, *209*, 2049.
[41] M. S. El-Genk, H. H. Saber, T. Caillat, J. Sakamoto, *Energy Convers. Manage.* **2006**, *47*, 174.
[42] M. S. El-Genk, H. H. Saber, *Energy Convers. Manage.* **2003**, *44*, 1069.
[43] M. S. El-Genk, H. H. Saber, T. Caillat, *Energy Convers. Manage.* **2003**, *44*, 1755.
[44] T. Caillat, J. P. Fleurial, G. J. Snyder, A. Borshchevsky, *Proc. 20th Inter. Conf. Thermoelectrics (ITC)* **2001**, 282.
[45] Q. Zhang, J. Liao, Y. Tang, M. Gu, C. Ming, P. Qiu, S. Bai, X. Shi, C. Uher, L. Chen, *Energy Environ. Sci.* **2017**, *10*, 956.
[46] D. Kraemer, Q. Jie, K. McEnaney, F. Cao, W. Liu, L. A. Weinstein, J. Loomis, Z. Ren, G. Chen, *Nat. Energy* **2016**, *1*, 16153.
[47] H. S. Kim, T. Wang, W. Liu, Z. Ren, *Adv. Funct. Mater.* **2016**, *26*, 3678.
[48] S. Leblanc, S. K. Yee, M. L. Scullin, C. Dames, K. E. Goodson, *Renewable Sustainable Energy Rev.* **2014**, *32*, 313.
[49] G. Schierning, R. Chavez, R. Schmechel, B. Balke, G. Rogl, P. Rogl, *Transl. Mater. Res.* **2015**, *2*, 025001.
[50] W. S. Liu, H. S. Kim, Q. Jie, Z. F. Ren, *Scipta Mater.* **2016**, *111*, 3.
[51] G. Joshi, R. He, M. Engber, G. Samsonidze, T. Pantha, E. Dahal, K. Dahal, J. Yang, Y. Lan, B. Kozinsky, Z. Ren, *Energy Environ. Sci.* **2014**, *7*, 4070.
[52] R. He, D. Kraemer, J. Mao, L. Zeng, Q. Jie, Y. Lan, C. Li, J. Shuai, H. S. Kim, Y. Liu, D. Broido, C.-W. Chu, G. Chen, Z. Ren, *Proc. Natl. Acad. Sci. USA* **2016**, *113*, 13576.
[53] S. K. Bux, R. G. Blair, P. K. Gogna, H. Lee, G. Chen, M. S. Dresselhaus, R. B. Kaner, J.-P. Fleurial, *Adv. Mater.* **2009**, *19*, 2445.
[54] G. Schierning, *Phys. Status Solidi A* **2014**, *211*, 1235.
[55] M. T. Barako, W. Park, A. M. Marconnet, M. Asheghi, K. E. Goodson, *J. Electron. Mater.* **2012**, *42*, 372.
[56] V. Kessler, M. Dehnen, R. Chavez, M. Engenhorst, J. Stoetzel, N. Petermann, K. Hesse, T. Huelser, M. Spree, C. Stiewe, P. Ziolkowski, G. Schierning, R. Schmechel, *J. Electron. Mater.* **2014**, *43*, 1389.
[57] N. N. Van, N. Pryds, *Adv. Nat. Sci.: Nanosci. Nanotechnol.* **2013**, *4*, 023002.
[58] W. Liu, Q. Jie, H. S. Kim, Z. Ren, *Acta Mater.* **2015**, *87*, 357.
[59] K. Biswas, J. He, I. D. Blum, C.-I. Wu, T. P. Hogan, D. N. Seidman, V. P. Dravid, M. G. Kanatzidis, *Nature* **2012**, *489*, 414.
[60] J. He, M. G. Kanatzidis, V. P. Dravid, *Mater. Today* **2013**, *16*, 166.
[61] H. Fateh, C. A. Baker, M. J. Hall, L. Shi, *Appl. Energy* **2014**, *129*, 373.
[62] M. Hodes, *IEEE Trans. Compon. Packag. Technol.* **2010**, *33*, 307.
[63] X. C. Xuan, K. C. Ng, C. Yap, H. T. Chua, *Energy Convers. Manage.* **2002**, *43*, 2041.
[64] S. Oki, R. O. Suzuki, *J. Electron. Mater.* **2017**, *46*, 2691.
[65] H. Ali, A. Z. Sahin, B. S. Yilbas, *Energy Convers. Manage.* **2014**, *78*, 634.
[66] B. S. Yilbas, H. Ali, *Energy Convers. Manage.* **2015**, *100*, 138.
[67] Y. Shi, D. Mei, Z. Yao, Y. Wang, H. Liu, Z. Chen, *Energy Convers. Manage.* **2015**, *97*, 1.
[68] A. Fabián-Mijangos, G. Min, J. Alvarez-Quintana, *Energy Convers. Manage.* **2017**, *148*, 1372.
[69] F. Stabler, presented at *DOE Thermoelectric Applications Workshop*, San Diego, CA, (accessed: January 2011).
[70] GMZ Energy Announces 1,000 Watt High-Temperature Thermoelectric Generator for U.S. Military. http://www.businesswire.com/multimedia/home/20141203005186/en/.
[71] F. Stabler, presented at *DOE Thermoelectric Applications Workshop on Future Tech LLC*, San Diego, CA (accessed: September–October 2009).
[72] C. Suter, P. Tomes, A. Steinfeld, A. Weidenkaff, *Materials* **2010**, *3*, 2735.
[73] P. Tomes, M. Trottmann, C. Suter, M. H. Aguirre, A. Steinfeld, P. Haueter, A. Weidenkaff, *Materials* **2010**, *3*, 2801.
[74] C. Suter, P. Tomeš, A. Weidenkaff, A. Steinfeld, *Sol. Energy* **2011**, *85*, 1511.
[75] P. Tomeš, C. Suter, M. Trottmann, A. Steinfeld, A. Weidenkaff, *J. Mater. Res.* **2011**, *26*, 1975.
[76] A. Weidenkaff, M. Trottmann, P. Tomes, C. Suter, A. Steinfeld, A. Veziridis, in *Materials Design and Applications*, Vol. *182* (Eds: K. Koumoto, T. Mori), Springer, Heidelberg **2013**, pp 365–382.
[77] D. Kraemer, B. Poudel, H. P. Feng, J. C. Caylor, B. Yu, X. Yan, Y. Ma, X. Wang, D. Wang, A. Muto, K. McEnaney, M. Chiesa, Z. Ren, G. Chen, *Nat. Mater.* **2011**, *10*, 532.
[78] M. L. Olsen, E. L. Warren, P. A. Parilla, E. S. Toberer, C. E. Kennedy, G. J. Snyder, S. A. Firdosy, B. Nesmith, A. Zakutayev, A. Goodrich, C. S. Turchi, J. Netter, M. H. Gray, P. F. Ndione, R. Tirawat, L. L. Baranowski, A. Gray, D. S. Ginley, *Energy Procedia* **2014**, *49*, 1460.
[79] I. Terasaki, R. Okazaki, P. S. Mondal, Y.-C. Hsieh, *Renewable Sustainable Energy Rev.* **2014**, *3*, 29.
[80] R. Komatsu, A. Balcytis, G. Seniutinas, T. Yamamura, Y. Nishijima, S. Juodkazis, *Sol. Energy Mater. Sol. Cells* **2015**, *143*, 72.
[81] R. Okazaki, A. Horikawa, Y. Yasui, I. Terasaki, *J. Phys. Soc. Jpn.* **2012**, *81*, 114722.
[82] G. Min, Thermoelectric Module Design Theories, in *Thermoelectrics Handbook: Macro to Nano*, (Ed.: D. M. Rowe), CRC Press, Boca Raton, FL **2005**.
[83] G. Min, D. M. Rowe, *Semicond. Sci. Technol.* **2007**, *22*, 880.
[84] A. Schmitz, C. Stiewe, E. Müller, *J. Electron. Mater.* **2013**, *42*, 1702.
[85] V. Jovovic, *Thermoelectric Waste Heat Recovery Program for Passenger Vehicles*, Gentherm Incorporated, Azusa, CA, USA **2015**, https://doi.org/10.2172/1337561.
[86] J. P. Fleurial, G. J. Snyder, J. A. Herman, P. H. Giauque, W. M. Phillips, M. A. Ryan, P. Shakkottai, E. A. Kolawa, M. A. Nicolet, in *Eighteenth Int. Conf. on Thermoelectrics*, IEEE, Piscataway, New Jersey **1999**, pp. 294–300.
[87] J. P. Fleurial, A. Borshchevsky, M. A. Ryan, W. Phillips, E. Kolawa, T. Kacisch, R. Ewell, in *XVI Int. Conf. on Thermoelectrics*, IEEE, Piscataway, New Jersey **1997**, pp. 641–645.
[88] R. Enright, S. Lei, K. Nolan, I. Mathews, A. Shen, G. Levaufre, R. Frizzell, G. H. Duan, D. Hernon, *Bell Labs Tech. J.* **2014**, *19*, 31.
[89] A. Shakouri, Z. Yan, *IEEE Trans. Compon. Packag. Technol.* **2005**, *28*, 65.
[90] J. Cancheevaram, R. Alley, E. Siivola, R. Venkatasubramanian, *MRS Online Proc. Libr.* **2004**, *793*, S8.18.1.
[91] V. Semeniouk, J. P. Fleurial, in *XVI Int. Conf. on Thermoelectrics*, IEEE, Piscataway, New Jersey **1997**, pp. 683–686.
[92] R. Yang, G. Chen, A. Ravi Kumar, G. J. Snyder, J.-P. Fleurial, *Energy Convers. Manage.* **2005**, *46*, 1407.
[93] Y. Ezzahri, S. Dilhaire, L. D. Patiño-Lopez, S. Grauby, W. Claeys, Z. Bian, Y. Zhang, A. Shakouri, *Superlattices Microstr.* **2007**, *41*, 7.
[94] C. Schumacher, K. G. Reinsberg, L. Akinsinde, S. Zastrow, S. Heiderich, W. Toellner, G. Rampelberg, C. Detavernier,

 © 2017 WILEY-VCH Verlag GmbH & Co. KGaA, Weinheim

J. A. C. Broekaert, K. Nielsch, J. Bachmann, *Adv. Energy Mater.* **2012**, *2*, 345.
[95] B. Y. Yoo, C. K. Huang, J. R. Lim, J. Herman, M. A. Ryan, J. P. Fleurial, N. V. Myung, *Electrochim. Acta* **2005**, *50*, 4371.
[96] R. Roth, R. Rostek, K. Cobry, C. Kohler, M. Groh, P. Woias, *J. Microelectromech. Syst.* **2014**, *23*, 961.
[97] G. J. Snyder, J. R. Lim, C. K. Huang, J. P. Fleurial, *Nat. Mater.* **2003**, *2*, 528.
[98] W. Glatz, E. Schwyter, L. Durrer, C. Hierold, *J. Microelectromech. Syst.* **2009**, *18*, 763.
[99] W. Glatz, S. Muntwyler, C. Hierold, *Sens. Actuators, A* **2006**, *132*, 337.
[100] R. Enright, S. Lei, I. Mathews, G. Cunningham, R. Frizzell, A. Shen, *ECS Trans.* **2015**, *69*, 37.
[101] U. Pelz, J. Jaklin, R. Rostek, M. Kröner, P. Woias, *J. Phys.: Conf. Ser.* **2015**, *660*, 012084.
[102] J. Garcia, D. A. L. Ramos, M. Mohn, H. Schlörb, N. P. Rodriguez, L. Akinsinde, K. Nielsch, G. Schierning, H. Reith, *ECS J. Solid State Sci. Technol.* **2017**, *6*, N3022.
[103] D. J. Yao, C. J. Kim, G. Chen, J. L. Liu, K. L. Wang, J. Snyder, J. P. Fleurial, in *20 Int. Conf. on Thermoelectrics*, IEEE, Piscataway, New Jersey **2001**, pp. 401–404.
[104] M. Kishi, H. Nemoto, T. Hamao, M. Yamamoto, S. Sudou, M. Mandai, S. Yamamoto, in *Eighteenth Int. Conf. on Thermoelectrics*, IEEE, Piscataway, New Jersey **1999**, pp. 301–307.
[105] H. Boettner, J. Nurnus, A. Gavrikov, G. Kuhner, M. Jagle, C. Kunzel, D. Eberhard, G. Plescher, A. Schubert, K. H. Schlereth, *J. Microelectromech. Syst.* **2004**, *13*, 414.
[106] M. Strasser, R. Aigner, M. Franosch, G. Wachutka, *Sens. Actuators, A* **2002**, *97*, 535.
[107] P. H. Kao, P. J. Shih, C. L. Dai, M. C. Liu, *Sensors* **2010**, *10*, 1315.
[108] M. Z. Yang, C. C. Wu, C. L. Dai, W. J. Tsai, *Sensors* **2013**, *13*, 2359.
[109] S. W. Peng, P. J. Shih, C. L. Dai, *Micromachines* **2015**, *6*, 1560.
[110] M. Stordeur, G. Willers, in *2nd European Conf. on Thermoelectrics*, European Thermoelectric Society, Krakow, Poland, **2004**.
[111] T. Huesgen, P. Woias, N. Kockmann, *Sens. Actuators, A* **2008**, *145*, 423.
[112] J. Su, R. J. M. Vullers, M. Goedbloed, Y. van Andel, R. Pellens, C. Gui, V. Leonov, Z. Wang, in *Proc. PowerMEMS 2008+ microEMS2008*, Sendai, Japan, **2008**, pp. 365–368.
[113] J. Su, V. Leonov, M. Goedbloed, Y. Van Andel, M. C. De Nooijer, R. Elfrink, Z. Wang, R. J. M. Vullers, *J. Micromech. Microeng.* **2010**, *20*, 104005.
[114] H. Glosch, M. Ashauer, U. Pfeiffer, W. Lang, *Sens. Actuators, A* **1999**, *74*, 246.
[115] I. Stark, *Planar thermoelectric generator*, US20110094556 A1, **2011**.
[116] M. Strasser, R. Aigner, C. Lauterbach, T. F. Sturm, M. Franosh, G. Wachutka, *Sens. Actuators A: Phys.*, **2004**, *114*, 362.
[117] M. Orrill, S. LeBlanc, *J. Appl. Polym. Sci.* **2016**, *134*, 44256.
[118] T. N. Huu, N. V. Toan, T. Ono, in *16th Int. Conf. on Nanotechnology (IEEE-NANO)*, IEEE, Piscataway, New Jersey **2016**, pp. 423–425.
[119] Y. Chen, Y. Zhao, Z. Liang, *Energy Environ. Sci.* **2015**, *8*, 401.
[120] R. Kroon, D. A. Mengistie, D. Kiefer, J. Hynynen, J. D. Ryan, L. Yu, C. Muller, *Chem. Soc. Rev.* **2016**, *45*, 6147.
[121] J. H. Bahk, H. Y. Fang, K. Yazawa, A. Shakouri, *J. Mater. Chem. C* **2015**, *3*, 10362.
[122] F. Suarez, A. Nozariasbmarz, D. Vashaee, M. C. Ozturk, *Energy Environ. Sci.* **2016**, *9*, 2099.
[123] B. Russ, A. Glaudell, J. J. Urban, M. L. Chabinyc, R. A. Segalman, *Nat. Rev. Mater.* **2016**, *1*, 16050.
[124] O. Bubnova, Z. U. Khan, A. Malti, S. Braun, M. Fahlman, M. Berggren, X. Crispin, *Nat. Mater.* **2011**, *10*, 429.
[125] O. Bubnova, Z. U. Khan, H. Wang, S. Braun, D. R. Evans, M. Fabretto, P. Hojati-Talemi, D. Dagnelund, J.-B. Arlin, Y. H. Geerts, S. Desbief, D. W. Breiby, J. W. Andreasen, R. Lazzaroni, W. M. Chen, I. Zozoulenko, M. Fahlman, P. J. Murphy, M. Berggren, X. Crispin, *Nat. Mater.* **2014**, *13*, 190.
[126] C. Cho, K. L. Wallace, P. Tzeng, J. H. Hsu, C. Yu, J. C. Grunlan, *Adv. Energy Mater.* **2016**, *6*, 1502168.
[127] C. Cho, B. Stevens, J.-H. Hsu, R. Bureau, D. A. Hagen, O. Regev, C. Yu, J. C. Grunlan, *Adv. Mater.* **2015**, *27*, 2996.
[128] Y. M. Sun, P. Sheng, C. A. Di, F. Jiao, W. Xu, D. Qiu, D. B. Zhu, *Adv. Mater.* **2012**, *24*, 932.
[129] N. Toshima, K. Oshima, H. Anno, T. Nishinaka, S. Ichikawa, A. Iwata, Y. Shiraishi, *Adv. Mater.* **2015**, *27*, 2246.
[130] F. Jiao, C. A. Di, Y. M. Sun, P. Sheng, W. Xu, D. B. Zhu, *Philos. Trans. R. Soc., A* **2014**, *372*, 20130008.
[131] B. Russ, M. J. Robb, F. G. Brunetti, P. L. Miller, E. E. Perry, S. N. Patel, V. Ho, W. B. Chang, J. J. Urban, M. L. Chabinyc, C. J. Hawker, R. A. Segalman, *Adv. Mater.* **2014**, *26*, 3473.
[132] Q. Yao, L. D. Chen, W. Q. Zhang, S. C. Liufu, X. H. Chen, *ACS Nano* **2010**, *4*, 2445.
[133] Y. Nonoguchi, M. Nakano, T. Murayama, H. Hagino, S. Hama, K. Miyazaki, R. Matsubara, M. Nakamura, T. Kawai, *Adv. Funct. Mater.* **2016**, *26*, 3021.
[134] D. D. Freeman, K. Choi, C. Yu, *PLoS One* **2012**, *7*, e47822.
[135] C. H. Yu, A. Murali, K. W. Choi, Y. Ryu, *Energy Environ. Sci.* **2012**, *5*, 9481.
[136] D. S. Montgomery, C. A. Hewitt, R. Barbalace, T. Jones, D. L. Carroll, *Carbon* **2016**, *96*, 778.
[137] H. Song, K. Cai, *Energy* **2017**, *125*, 519.
[138] Y. Yang, Z.-H. Lin, T. Hou, F. Zhang, Z. L. Wang, *Nano Res.* **2012**, *5*, 888.
[139] Y. Wang, S. M. Zhang, Y. Deng, *J. Mater. Chem. A* **2016**, *4*, 3554.
[140] Z. Antar, J. F. Feller, H. Noel, P. Glouannec, K. Elleuch, *Mater. Lett.* **2012**, *67*, 210.
[141] Y. C. Sun, D. Terakita, A. C. Tseng, H. E. Naguib, *Smart Mater. Struct.* **2015**, 24.
[142] M. Liebscher, T. Gartner, L. Tzounis, M. Micusik, P. Potschke, M. Stamm, G. Heinrich, B. Voit, *Compos. Sci. Technol.* **2014**, *101*, 133.
[143] L. Tzounis, T. Gartner, M. Liebscher, P. Potschke, M. Stamm, B. Voit, G. Heinrich, *Polymer* **2014**, *55*, 5381.
[144] H. Pang, Y. Y. Piao, Y. Q. Tan, G. Y. Jiang, J. H. Wang, Z. M. Li, *Mater. Lett.* **2013**, *107*, 150.
[145] J. Luo, B. Krause, P. Pötschke, *AIMS Mater. Sci.* **2016**, *3*, 1107.
[146] P. Aranguren, A. Roch, L. Stepien, M. Abt, M. von Lukowicz, I. Dani, D. Astrain, *Appl. Therm. Eng.* **2016**, *102*, 402.
[147] M. Culebras, C. Cho, M. Krecker, R. Smith, Y. Song, C. M. Gómez, A. Cantarero, J. C. Grunlan, *ACS Appl. Mater. Interfaces* **2017**, *9*, 6306.
[148] C. J. An, Y. H. Kang, A. Y. Lee, K.-S. Jang, Y. Jeong, S. Y. Cho, *ACS Appl. Mater. Interfaces* **2016**, *8*, 22142.
[149] S. L. Kim, K. Choi, A. Tazebay, C. Yu, *ACS Nano* **2014**, *8*, 2377.
[150] W. Zhou, Q. Fan, Q. Zhang, L. Cai, K. Li, X. Gu, F. Yang, N. Zhang, Y. Wang, H. Liu, W. Zhou, S. Xie, *Nat. Commun.* **2017**, *8*, 14886.
[151] J. Choi, Y. Jung, S. J. Yang, J. Y. Oh, J. Oh, K. Jo, J. G. Son, S. E. Moon, C. R. Park, H. Kim, *ACS Nano* **2017**, *11*, 7608.
[152] J. Choi, J. Y. Lee, S.-S. Lee, C. R. Park, H. Kim, *Adv. Energy Mater.* **2016**, *6*, 1502181.
[153] J. Lee, H. J. Kim, S. Oh, S. H. Choi, V. K. Varadan, *Proc. SPIE* **2012**, *8344*, 83440H.
[154] Z. Cao, M. J. Tudor, R. N. Torah, S. P. Beeby, *IEEE Trans. Electron Devices* **2016**, *63*, 4024.
[155] D. Madan, A. Chen, P. K. Wright, J. W. Evans, *J. Appl. Phys.* **2011**, *109*, 034904.
[156] D. Madan, Z. Wang, A. Chen, R. Winslow, P. K. Wright, J. W. Evans, *Appl. Phys. Lett.* **2014**, *104*, 013902.

 © 2017 WILEY-VCH Verlag GmbH & Co. KGaA, Weinheim

[157] J. H. We, S. J. Kim, B. J. Cho, *Energy* **2014**, *73*, 506.
[158] E. Jin Bae, Y. Hun Kang, K.-S. Jang, S. Yun Cho, *Sci. Rep.* **2016**, *6*, 18805.
[159] S. J. Kim, H. Choi, Y. Kim, J. H. We, J. S. Shin, H. E. Lee, M.-W. Oh, K. J. Lee, B. J. Cho, *Nano Energy* **2017**, *31*, 258.
[160] T. Zhang, K. Li, C. Li, S. Ma, H. H. Hng, L. Wei, *Adv. Electron. Mater.* **2017**, *3*, 1600554.
[161] S. H. Park, S. Jo, B. Kwon, F. Kim, H. W. Ban, J. E. Lee, D. H. Gu, S. H. Lee, Y. Hwang, J.-S. Kim, D.-B. Hyun, S. Lee, K. J. Choi, W. Jo, J. S. Son, *Nat. Commun.* **2016**, *7*, 13403.
[162] Z. Lu, H. Zhang, C. Mao, C. M. Li, *Appl. Energy* **2016**, *164*, 57.
[163] C. Wan, R. Tian, A. B. Azizi, Y. Huang, Q. Wei, R. Sasai, S. Wasusate, T. Ishida, K. Koumoto, *Nano Energy* **2016**, *30*, 840.
[164] C. Wan, X. Gu, F. Dang, T. Itoh, Y. Wang, H. Sasaki, M. Kondo, K. Koga, K. Yabuki, G. J. Snyder, R. Yang, K. Koumoto, *Nat. Mater.* **2015**, *14*, 622.
[165] J. Y. Oh, J. H. Lee, S. W. Han, S. S. Chae, E. J. Bae, Y. H. Kang, W. J. Choi, S. Y. Cho, J.-O. Lee, H. K. Baik, T. I. Lee, *Energy Environ. Sci.* **2016**, *9*, 1696.
[166] J. Weber, K. Potje-Kamloth, F. Haase, P. Detemple, F. Völklein, T. Doll, *Sens. Actuators, A* **2006**, *132*, 325.
[167] Z. Lu, M. Layani, X. Zhao, L. P. Tan, T. Sun, S. Fan, Q. Yan, S. Magdassi, H. H. Hng, *Small* **2014**, *10*, 3551.
[168] K. Suemori, S. Hoshino, T. Kamata, *Appl. Phys. Lett.* **2013**, *103*, 153902.
[169] F. Zhang, Y. Zang, D. Huang, C.-a. Di, D. Zhu, *Nat. Commun.* **2015**, *6*, 8356.
[170] B. Russ, A. M. Glaudell, J. J. Urban, M. L. Chabinyc, R. A. Segalman, *Nat. Rev. Mater.* **2016**, *1*, 16050.
[171] Y. He, T. Day, T. Zhang, H. Liu, X. Shi, L. Chen, G. J. Snyder, *Adv. Mater.* **2014**, *26*, 3974.
[172] K. T. Settaluri, H. Lo, R. J. Ram, *J. Electron. Mater.* **2012**, *41*, 984.
[173] V. Leonov, *IEEE Sens. J.* **2013**, *13*, 2284.
[174] S. Lv, W. He, L. Wang, G. Li, J. Ji, H. Chen, G. Zhang, *Appl. Therm. Eng.* **2016**, *109*, 138.
[175] M. Wahbah, M. Alhawari, B. Mohammad, H. Saleh, M. Ismail, *IEEE J. Emerging Sel. Top. Circuits Syst.* **2014**, *4*, 354.
[176] L. Francioso, C. De Pascali, V. Sglavo, A. Grazioli, M. Masieri, P. Siciliano, *Energy Convers. Manage.* **2017**, *145*, 204.
[177] H. Liu, Y. Wang, D. Mei, Y. Shi, Z. Chen, in *Proc. of Int. Conf. on Wearable Sensors and Robots 2015* (Eds: C. Yang, G. S. Virk, H. Yang), Springer,Singapore **2017**, pp 55–66.
[178] K. Pietrzyk, J. Soares, B. Ohara, H. Lee, *Appl. Energy* **2016**, *183*, 218.
[179] A. R. M. Siddique, S. Mahmud, B. V. Heyst, *Renewable Sustainable Energy Rev.* **2017**, *73*, 730.
[180] V. Leonov, R. J. M. Vullers, *J. Electron. Mater.* **2009**, *38*, 1491.
[181] R. F. Hartman, C. E. Kelly, *AIP Conf. Proc.* **1993**, *271*, 301.
[182] A. A. Zakhidov, Y. I. Ravich, D. A. Pchenoy-Severin, in *Eighteenth Int. Conf. on Thermoelectrics*, IEEE, Piscataway, New Jersey **1999**, pp. 193–197.
[183] F. Volklein, W. Wittmer, U. Birkholz, *Energy Convers. Manage.* **1993**, *34*, 687.
[184] U. Stohrer, R. Voggesberger, G. Wagner, U. Birkholz, *Energy Convers. Manage.* **1990**, *30*, 143.
[185] R. Chavez, S. Angst, J. Hall, F. Maculewicz, J. Stötzel, H. Wiggers, T. Hung Le, N. N. Van, N. Pryds, G. Span, D. Wolf, R. Schmechel, G. Schierning, *J. Phys. D: Applied Physics* **2017**, https://doi.org/10.1088/1361-6463/aa9b6a.
[186] M. Wagner, G. Span, S. Holzer, T. Grasser, *Semicond. Sci. Technol.* **2007**, *22*, S173.
[187] G. Span, M. Wagner, S. Holzer, T. Grasser, in *25th Int. Conf. on Thermoelectrics, ICT '06*, IEEE, Piscataway, New Jersey **2006**, pp. 23–28.
[188] S. Funahashi, H. Guo, J. Guo, A. L. Baker, K. Wang, K. Shiratsuyu, C. A. Randall, *J. Am. Ceram. Soc.* **2017**, *100*, 3488.
[189] S. A. Ali, S. Mazumder, *Int. J. Heat Mass Transfer* **2013**, *62*, 373.
[190] S. Teichert, A. Bochmann, T. Reimann, T. Schulz, C. Dreßler, S. Udich, J. Töpfer, *J. Electron. Mater.* **2016**, *45*, 1966.
[191] S. Teichert, A. Bochmann, T. Reimann, T. Schulz, C. Dreßler, J. Töpfer, *AIP Adv.* **2015**, *5*, 077105.
[192] A. Sakai, T. Kanno, K. Takahashi, H. Tamaki, H. Kusada, Y. Yamada, H. Abe, *Sci. Rep.* **2014**, *4*, 6089.
[193] T. Kanno, S. Yotsuhashi, A. Sakai, K. Takahashi, H. Adachi, *Appl. Phys. Lett.* **2009**, *94*, 061917.
[194] C. Reitmaier, F. Walther, H. Lengfellner, *Appl. Phys. A* **2010**, *99*, 717.
[195] Y. Shiomi, Y. Handa, T. Kikkawa, E. Saitoh, *Appl. Phys. Lett.* **2015**, *106*, 232403.
[196] L. Yu, Y. Wang, P. Zhang, H.-U. Habermeier, *Phys. Status Solidi RRL* **2013**, *7*, 180.
[197] G. Yan, Z. Bai, S. Wang, L. Sun, J. Wang, G. Fu, *Appl. Opt.* **2014**, *53*, 4211.
[198] H. Lengfellner, G. Kremb, A. Schnellbögl, J. Betz, K. F. Renk, W. Prettl, *Appl. Phys. Lett.* **1992**, *60*, 501.
[199] H.-H. Huang, M.-P. Lu, C.-N. Liao, *J. Appl. Phys.* **2016**, *119*, 205101.
[200] C. Zhou, S. Birner, Y. Tang, K. Heinselman, M. Grayson, *Phys. Rev. Lett.* **2013**, *110*, 227701.
[201] K. Takahashi, T. Kanno, A. Sakai, H. Tamaki, H. Kusada, Y. Yamada, **2013**, *3*, 1501.
[202] H. J. Goldsmid, *J. Electron. Mater.* **2011**, *40*, 1254.
[203] D. Ebling, K. Bartholomé, M. Bartel, M. Jägle, *J. Electron. Mater.* **2010**, *39*, 1376.
[204] V. Ravi, S. Firdosy, T. Caillat, E. Brandon, K. Van Der Walde, L. Maricic, A. Sayir, *J. Electron. Mater.* **2009**, *38*, 1433.
[205] G. Rogl, A. Grytsiv, M. Gürth, A. Tavassoli, C. Ebner, A. Wünschek, S. Puchegger, V. Soprunyuk, W. Schranz, E. Bauer, H. Müller, M. Zehetbauer, P. Rogl, *Acta Mater.* **2016**, *107*, 178.
[206] S. K. Thakur, B. K. Dhindaw, N. Hort, K. U. Kainer, *Metall. Mater. Trans. A* **2004**, *35*, 1167.
[207] M. S. Rogachev, L. M. Pavlova, Y. I. Shtern, *J. Phys.: Conf. Ser.* **2016**, *741*, 012203.
[208] L. Pavlova, Y. Shtern, E. Kirilenko, *J. Mater. Sci.* **2016**, *52*, 921.
[209] R. D. Schmidt, E. D. Case, J. E. Ni, J. S. Sakamoto, R. M. Trejo, E. Lara-Curzio, E. A. Payzant, M. J. Kirkham, R. A. Peascoe-Meisner, *Philos. Mag.* **2012**, *92*, 1261.
[210] D. Zhao, H. Geng, X. Teng, *J. Alloys Compd.* **2012**, *517*, 198.
[211] J.-L. Gao, Q.-G. Du, X.-D. Zhang, X.-Q. Jiang, *J. Electron. Mater.* **2011**, *40*, 884.
[212] A. S. Al-Merbati, B. S. Yilbas, A. Z. Sahin, *Appl. Therm. Eng.* **2013**, *50*, 683.
[213] H. Xia, F. Drymiotis, C.-L. Chen, A. Wu, G. J. Snyder, *J. Mater. Sci.* **2013**, *49*, 1716.
[214] K. Kishimoto, M. Tsukamoto, T. Koyanagi, *J. Appl. Phys.* **2002**, *92*, 5331.
[215] F. Ren, B. D. Hall, E. D. Case, E. J. Timm, R. M. Trejo, R. A. Meisner, E. Lara-Curzio, *Philos. Mag.* **2009**, *89*, 1439.
[216] N. L. Okamoto, T. Nakano, K. Tanaka, H. Inui, *J. Appl. Phys.* **2008**, *104*, 013529.
[217] A. Singh, S. Bhattacharya, C. Thinaharan, D. K. Aswal, S. K. Gupta, J. V. Yakhmi, K. Bhanumurthy, *J. Phys. D: Appl. Phys.* **2009**, *42*, 015502.
[218] X. Shan, R. Huang, Y. Han, C. Huang, X. Liu, Z. Lu, L. Li, *J. Alloys Compd.* **2016**, *662*, 505.
[219] W. Liu, H. Wang, L. Wang, X. Wang, G. Joshi, G. Chen, Z. Ren, *J. Mater. Chem. A* **2013**, *1*, 13093.
[220] C. C. Li, F. Drymiotis, L. L. Liao, H. T. Hung, J. H. Ke, C. K. Liu, C. R. Kao, G. J. Snyder, *J. Mater. Chem. C* **2015**, *3*, 10590.
[221] D. Zhao, H. Geng, L. Chen, *Int. J. Appl. Ceram. Technol.* **2012**, *9*, 733.

© 2017 WILEY-VCH Verlag GmbH & Co. KGaA, Weinheim

[222] D. Zhao, X. Li, L. He, W. Jiang, L. Chen, *J. Alloys Compd.* **2009**, *477*, 425.
[223] V. M. Sokolova, L. D. Dudkin, L. I. Petrova, *Inorg. Mater.* **2000**, *36*, 16.
[224] Y. S. Ju, U. Ghoshal, *J. Appl. Phys.* **2000**, *88*, 4135.
[225] O. Yamashita, *Appl. Energy* **2011**, *88*, 3022.
[226] M. Mantelli, M. Yovanovich, Thermal contact resistance, in *Spacecraft Thermal Control Handbook*, (Ed.: D. Gilmore), The Aerospace Press, El Segundo, California **2002**.
[227] E. T. Swartz, R. O. Pohl, *Rev. Mod. Phys.* **1989**, *61*, 605.
[228] T. S. English, J. C. Duda, J. L. Smoyer, D. A. Jordan, P. M. Norris, L. V. Zhigilei, *Phys. Rev. B* **2012**, *85*, 035438.
[229] S. M. Sze, *Semiconductor Devices: Physics and Technology*. John Wiley & Sons, New York **2008**.
[230] H. Lüth, *Solid Surfaces, Interfaces and Thin Films*, 5th ed., 2010, Springer, Heidelberg Dordrecht, London, New York **2010**, pp. 377–433.
[231] E. Rhoderick, R. Williams, *Monographs in Electrical and Electronic Engineering*, Oxford University Press, Oxford, England **1988**.
[232] J. Bardeen, *Phys. Rev.* **1947**, *71*, 717.
[233] V. L. Rideout, *Solid-State Electron.* **1975**, *18*, 541.
[234] S. Kurtin, T. C. McGill, C. A. Mead, *Phys. Rev. Lett.* **1969**, *22*, 1433.
[235] D.-G. Zhao, J. W. Lixy, *J. Inorg. Mater.* **2009**, *24*, 545.
[236] T. Caillat, J.-P. Fleurial, G. Snyder, A. Borshchevsky, in *MRS Proc.*, Cambridge Univ Press, Warrendale, Pennsylvania **2000**, p. Z11. 6.
[237] J. P. Fleurial, T. Caillat, S. C. Chi, *US 20120006376 A1*, **2012**.
[238] J. Q. Guo, H. Y. Geng, T. Ochi, S. Suzuki, M. Kikuchi, Y. Yamaguchi, S. Ito, *J. Electron. Mater.* **2012**, *41*, 1036.
[239] A. Muto, J. Yang, B. Poudel, Z. Ren, G. Chen, *Adv. Energy Mater.* **2013**, *3*, 245.
[240] Q. JIE, Z. Ren, G. Chen, *US 9722164 B2*, **2015**.
[241] G. Bennett, J. Lombardo, R. Hemler, G. Silverman, C. Whitmore, W. Amos, E. Johnson, A. Schock, R. Zocher, T. Keenan, in *4th International Energy Conversion Engineering Conference and Exhibit (IECEC)*, The American Institute of Aeronautics and Astronautics, Reston, VA **2006**, p. 4096.
[242] J. S. Lin, K. Tanihata, Y. Miyamoto, H. Kido, *Functionally Graded Materials 1996, Proceedings of the 4th International Symposium on Functionally Graded Materials*, (Eds.: I. Shiota, Y. Miyamoto), Elsevier, **1997**, pp. 599–604, https://doi.org/10.1016/b978-044482548-3/50098-6.
[243] J.-S. Lin, Y. Miyamoto, *J. Mater. Res.* **2011**, *15*, 647.
[244] X. Y. Yang, J. H. Wu, M. Gu, X. G. Xia, L. D. Chen, *Ceram. Int.* **2016**, *42*, 8044.
[245] D.-W. Liu, J.-F. Li, C. Chen, B.-P. Zhang, L. Li, *J. Micromech. Microeng.* **2010**, *20*, 125031.
[246] S.-P. Feng, Y.-H. Chang, J. Yang, B. Poudel, B. Yu, Z. Ren, G. Chen, *Phys. Chem. Chem. Phys.* **2013**, *15*, 6757.
[247] T. Y. Lin, C. N. Liao, A. T. Wu, *J. Electron. Mater.* **2011**, *41*, 153.
[248] W. P. Lin, D. E. Wesolowski, C. C. Lee, *J. Mater. Sci.: Mater. Electron.* **2011**, *22*, 1313.
[249] L. W. da Silva, M. Kaviany, *J. Microelectromech. Syst.* **2005**, *14*, 1110.
[250] N. Van Nong, T. H. Le, L. Han, H. N. Pham, N. Pryds, in *34th Annual International Conference on Thermoelectrics (ICT 2015) and 13th European Conference on Thermoelectrics (ECT 2015)*, **2015**.
[251] T. Kacsich, E. Kolawa, J. Fleurial, T. Caillat, M. Nicolet, *J. Phys. D: Appl. Phys.* **1998**, *31*, 2406.
[252] F. A. Leavitt, J. W. McCoy, P. Marudhachalam, M. Gaertner, *US 20120103381 A1*, **2012**.
[253] M. Orihashi, Y. Noda, L. Chen, Y. Kang, A. Moro, T. Hirai, *Proceedings of 17th International Conference on Thermoelectrics*, IEEE, Piscataway, New Jersey **1998**, p. 543, https://doi.org/10.1109/ICT.1998.740437.
[254] G. Joshi, J. Yang, M. Engber, T. Pantha, M. Cleary, Z. Ren, R. He, B. Kozinsky, *US 20150270465 A1*, **2015**.
[255] Y. Zhang, X. Wang, M. Cleary, L. Schoensee, N. Kempf, J. Richardson, *Appl. Therm. Eng.* **2016**, *96*, 83.

© 2017 WILEY-VCH Verlag GmbH & Co. KGaA, Weinheim